Nucleic Acids Research, 2024, **52**, 1814–1829
https://doi.org/10.1093/nar/gkad1224
Advance access publication date: 5 January 2024
Molecular Biology

Kaposi's sarcoma herpesvirus exploits the DNA damage response to circularize its genome

Shijun Li[1,2], Bing Liu[1,2], Min Tan[1,2], Franceline Juillard[1,2], Agnieszka Szymula[1,2], Ángel L. Álvarez[1,2], Nicholas Van Sciver[1,2], Athira George[1,2], Akshaya Ramachandran[1,2], Komal Raina[1,2], Vinayak Sadasivam Tumuluri[1,2], Catarina N. Costa[3,4], J. Pedro Simas[3,4,*] and Kenneth M. Kaye[1,2,5,*]

[1]Departments of Medicine, Brigham and Women's Hospital and Harvard Medical School, Boston, MA 02115, USA
[2]Program in Virology, Harvard Medical School, Boston, MA 02115, USA
[3]Instituto de Medicina Molecular, Faculdade de Medicina, Universidade de Lisboa, Avenida Professor Egas Moniz, 1649-028 Lisboa, Portugal
[4]Universidade Católica Portuguesa, Católica Medical School, Católica Biomedical Research, Palma de Cima, 1649-023 Lisboa, Portugal
[5]Broad Institute of Harvard University and Massachusetts Institute of Technology, Cambridge, MA 02142, USA

*To whom correspondence should be addressed. Tel: +1 617 525 4256; Email: kkaye@bwh.harvard.edu
Correspondence may also be addressed to J. Pedro Simas. Email: psimas@ucp.pt
Present address: Ángel L. Álvarez, Instituto Universitario de Biotecnología de Asturias (IUBA), University of Oviedo (Spain).

Abstract

To establish lifelong, latent infection, herpesviruses circularize their linear, double-stranded, DNA genomes through an unknown mechanism. Kaposi's sarcoma (KS) herpesvirus (KSHV), a gamma herpesvirus, is tightly linked with KS, primary effusion lymphoma, and multicentric Castleman's disease. KSHV persists in latently infected cells as a multi-copy, extrachromosomal episome. Here, we show the KSHV genome rapidly circularizes following infection, and viral protein expression is unnecessary for this process. The DNA damage response (DDR) kinases, ATM and DNA-PKcs, each exert roles, and absence of both severely compromises circularization and latency. These deficiencies were rescued by expression of ATM and DNA-PKcs, but not catalytically inactive mutants. In contrast, γH2AX did not function in KSHV circularization. The linear viral genomic ends resemble a DNA double strand break, and non-homologous DNA end joining (NHEJ) and homologous recombination (HR) reporters indicate both NHEJ and HR contribute to KSHV circularization. Last, we show, similar to KSHV, ATM and DNA-PKcs have roles in circularization of the alpha herpesvirus, herpes simplex virus-1 (HSV-1), while γH2AX does not. Therefore, the DDR mediates KSHV and HSV-1 circularization. This strategy may serve as a general herpesvirus mechanism to initiate latency, and its disruption may provide new opportunities for prevention of herpesvirus disease.

Graphical abstract

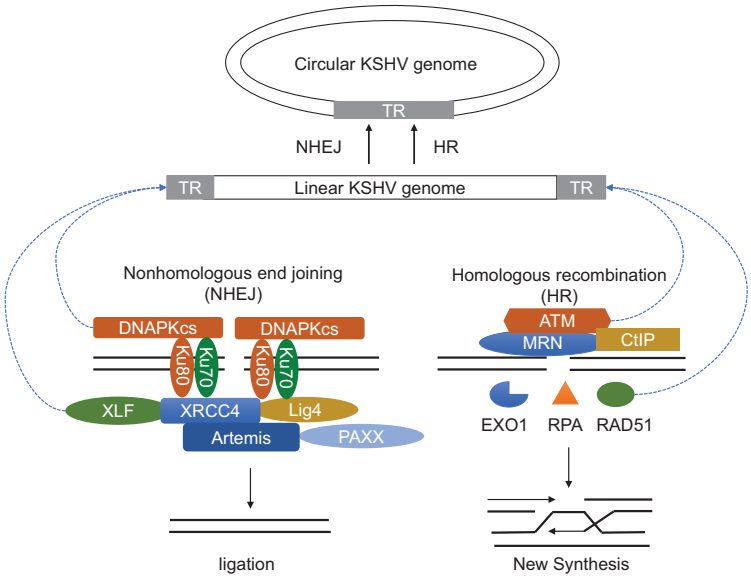

Received: October 16, 2023. **Revised:** December 5, 2023. **Editorial Decision:** December 8, 2023. **Accepted:** December 16, 2023

Introduction

Lifelong latency is a hallmark of herpesvirus infection, which occurs following circularization of the linear viral genomes (1). Latency is well characterized for gamma-herpesviruses. Kaposi's sarcoma herpesvirus (KSHV or HHV-8), a gamma-herpesvirus, is the etiologic agent of Kaposi's sarcoma (KS) and is associated with the lymphoproliferative disorders primary effusion lymphoma (PEL), and multicentric Castleman's disease (2–7). The KSHV virion is enveloped, and contains a ∼165 kb linear, double-stranded DNA genome encoding ∼100 genes. Upon latency establishment, the KSHV genome persists as a multicopy, extrachromosomal, circular episome (plasmid), including in tumor cells (8). During latency, the viral genome expresses a limited number of proteins, including the latency-associated nuclear antigen (LANA). The episomal DNA replicates with each cell cycle and LANA mediates its persistence by tethering genomes to mitotic chromosomes to segregate viral DNA to progeny cell nuclei (9–11).

The DNA damage response (DDR) is comprised of multiple cellular pathways that function to detect and repair DNA lesions. Important upstream mediators of the DDR include phosphatidylinositol 3-kinase like protein kinases (PIKKs). These include ATM (ataxia telangiectasia mutated), ATR (ataxia telangiectasia and Rad3-related), and DNA-PK (DNA-dependent protein kinase). Each of these kinases responds chiefly to a specific type of DNA damage (12). ATM and DNA-PK primarily respond to double strand DNA breaks (DSBs) whereas ATR responds to the presence of single-strand DNA. Homologous recombination (HR) and non-homologous DNA end joining (NHEJ) are two major mechanisms through which DSBs are repaired(13). Following DSBs, histone H2AX is phosphorylated by PIKKs at serine 139 to form γH2AX, which is present at chromatin surrounding the break, and serves as a platform for accumulation of DNA repair factors (14,15).

Virus infection introduces foreign nucleic acid into host cells, and often induces a DNA damage response (DDR). Accordingly, KSHV infection activates the DDR, as evidenced by elevated levels of phosphorylated γH2AX in the nuclei of infected cells (16). The KSHV induced DDR has been at least partially attributed to viral DNA replication and viral gene expression. In KS tumors, the DDR is activated in early lesions and is likely associated with robust cell proliferation (16–18). KSHV infection activates ATM, and γH2AX has been shown to localize to viral genomes. (19,20) KSHV viral interferon regulatory factor 1 (vIRF1) inhibits ATM kinase activity, but this gene is expressed only in the lytic phase of virus infection (21).

Although central to KSHV and herpesvirus biology, little is known regarding the processes governing genome circularization. In order for KSHV to circularize, the free DNA ends of its linear genome must be covalently fused. ATM and DNA-PK are activated to facilitate joining the free DNA ends at sites of DSBs on the host genome, but whether they are involved in linking the free DNA ends of the KSHV genome is not known. The linear KSHV genome is flanked by ∼40 tandem terminal repeats (TRs) arranged in a head-to-tail orientation, with each repeat consisting of 801 bp of GC-rich DNA (22–24). The presence of these TRs at the KSHV free ends suggest either NHEJ or HR could effect circularization of the viral genome.

Numerous studies have described the interactions between herpesvirus infection and cellular DDR pathways (25), but how the DDR might contribute to herpesvirus circularization is poorly understood. The mechanism(s) involved in either KSHV or Epstein-Barr virus (EBV) gamma herpesvirus circularization are unknown, while investigation of HSV-1 circularization is complicated by its predilection for permissive infection *in vitro*, during which circularization is undetectable by Southern blot due to expression of infected cell protein 0 (ICP0) (26).

In contrast to alpha herpesviruses, gamma herpesviruses have latency rather than lytic infection as their default program allowing circularization to be directly detected following infection. Here, we use KSHV as a model gamma herpesvirus to study the role of the DDR on viral genome circularization. We explored the effect of the apical DDR signaling kinases ATM and DNAPKcs, and other pathway specific DDR components including Rad51 in the HR pathway and XLF in the NHEJ pathway, on KSHV circularization. Our results show that ATM exerts a modest role, and DNAPK a larger role in KSHV circularization, and that absence of both these enzymes engenders severe circularization deficiency. In contrast, γH2AX does not have a role in circularization. We also extend our findings to show ATM and DNAPK have similar roles in circularization of ICP0 null HSV-1, suggesting a common mechanism for herpesvirus circularization.

Materials and methods

Cells

HEK293T (293T) cells were obtained from the American Type Culture Collection (Manassas, VA). SLK cells were obtained from the NIH AIDS Reagent Program. SLK and 293T cells were maintained at 37°C in Dulbecco's modified Eagle's medium (DMEM; Gibco-BRL) supplemented with 10% (vol/vol) bovine growth serum (BGS) (HyClone) and 15 μg/ml gentamicin. BJAB and BCBL-1 cells were cultured in RPMI 1640 medium (Gibco) supplemented with 10% (vol/vol) BGS and 15 μg/ml gentamicin. iSLK.219 cells are latently infected with a recombinant KSHV.219 (rKSHV.219) and carry integrated, doxycycline-inducible, KSHV replication transcription activator (RTA), and were maintained at 37°C in DMEM (Gibco) supplemented with 10% (vol/vol) BGS and 15 μg/ml gentamicin. In iSLK.219 cells, 10μg/ml puromycin in combination with 1 mg/ml G418 was used to maintain rKSHV.219 and the rtTA Tet-On transactivator, respectively. Human Dermal Microvascular Endothelial Cells (HDMVEC) (ATCC) were maintained at 37°C in Vascular Cell Basal Medium (ATCC PCS-100–030) supplemented with Microvascular Endothelial Cell Growth Kit-BBE (ATCC PCS-110-040) and 15 μg/ml gentamicin.

Plasmids and cloning

pcDNA3.1(+)Flag-His-ATM wt was a gift from Michael Kastan (Addgene plasmid # 31985; http://n2t.net/addgene:31985;RRID:Addgene_31985) (27). pcDNA3.1(+) Flag-His-ATM kd was a gift from Michael Kastan (Addgene plasmid # 31986; http://n2t.net/addgene:31986;RRID:Addgene_31986) (27). hu DNA-PKcs was a gift from Katheryn Meek (Addgene plasmid # 83317; http://n2t.net/addgene:83317;RRID:Addgene_83317)

(28). DNA-PKcs T3950D was a gift from Katheryn Meek (Addgene plasmid # 83320; http://n2t.net/addgene:83320;RRID:Addgene_83320) (29). LentiCRISPRv2 puro was a gift from Brett Stringer (Addgene plasmid # 98290; http://n2t.net/addgene:98290;RRID:Addgene_98290) (30). pLKO.1 puro was a gift from Bob Weinberg (Addgene plasmid # 8453; http://n2t.net/addgene:8453;RRID:Addgene_8453) (31). pCMV-VSV-G was a gift from Bob Weinberg (Addgene plasmid # 8454; http://n2t.net/addgene: 8454; RRID:Addgene_8454) (31). psPAX2 was a gift from Didier Trono (Addgene plasmid # 12260; http://n2t.net/addgene:12260;RRID:Addgene_12260). DsRed2-C1 was a gift from Michael Davidson (Addgene plasmid # 54611; http://n2t.net/addgene:54611;RRID:Addgene_54611). pEGFP-C1 (Clontech) was used to express green fluorescent protein (GFP).

Guide RNA sequences used for CRISPR, and shRNA sequences used for knockdown are listed in Supplementary Table S1. Each pair of guide RNA oligonucleotides were annealed and cloned into BsmBI digested LentiCRISPR v2 plasmid. Each pair of shRNA oligonucleotides were annealed and cloned into EcoRI and AgeI digested pLKO.1 puro plasmid.

The HR and NHEJ reporter plasmids were kindly provided by Vera Gorbunova at the University of Rochester (32). The NHEJ reporter cassette was cloned into pcDNA3.1(+) using restriction sites BamHI and NotI. The HR reporter cassette was cloned into pcDNA3.1(+) using restriction sites KpnI and XhoI.

Transfections

293T cells were transfected with Lipofectamine 3000 transfection kit (L3000015, Invitrogen) following the manufacturer's instructions. BJAB cells were transfected by electroporation using the Neon Transfection System (MPK5000, Thermo Fisher Scientific) following the manufacturer's instructions. The setting for electroporation was pulse voltage: 1350V, pulse width: 40ms and Pulse number: 1.

Generation of knockout, knockdown, or gene reconstituted cell lines

We targeted ATM, DNAPKcs or H2AX for using CRISPR/Cas9 in 293T cells. 1×10^6 293T cells were transfected with 0.5 μg of lentiCRISPR v2 plasmid expressing a gene specific guide RNA (Supplementary Table S1) using lipofectamine 3000 (L3000015, Invitrogen) per the manufacturer's protocol. Twenty-four hours post transfection, cells were placed under 1μg/ml of puromycin selection, for which resistance is encoded by the plasmid, for 48 ho to kill the non-transfected cells. Next, 1000 cells were seeded into 150 mm plates, and cells cultured in medium without puromycin for 2–3 weeks to allow colony formation. Cells were expanded from different colonies, and tested by western blot to assess for knockout of the targeted genes. DNAPKcs was also targeted in ATM knockout cells to generate ATM/DNAPKcs double knockout cells.

To generate Rad51 or XLF knockdown cells, lentivirus expressing Rad51 or XLF shRNA (Supplementary Table S1) was used to transduce 293T cells. 293T cells in 6-well plates at 70% confluence were incubated with 1ml of lentivirus expressing Rad51, XLF, or control shRNA for 24 h and medium was then supplemented with 1 μg/ml puromycin to allow selection of transduced cells. After 2 days of puromycin selection, the pooled cells were assessed for Rad51 or XLF knockdown by immunoblot and used in experiments. Rad51 is an essential gene, so knockouts cannot be generated, and in fact, lentivirus Rad51 shRNA transduced cells ceased growing well after 4–5 days of puromycin selection. After continued puromycin selection, cells began to grow out after about one week. This later outgrowth resulted only in cells expressing Rad51 at wild type levels. As a result, transiently transduced cells were used for these experiments.

To reconstitute ATM or DNAPKcs expression in knockout cells, pcDNA3.1(+)Flag-His-ATM wt, pcDNA3.1(+) Flag-His-ATM kd, hu DNA-PKcs, DNA-PKcs T3950D was transfected into cells using lipofectamine 3000 as above to express ATM, ATM kd (catalytically inactive ATM), DNAPKcs or DNA-PKcs T3950D (catalytically inactive DNA-PKcs.) Twenty-four hours following transfection, cells were infected with rKSHV.219 MOI ∼3.

Bleomycin treatment

To assess the DDR, 293T, SLK or HDMVEC cells were incubated with 5 μM of bleomycin (Santa Cruz Biotechnology, sc-200134) for 30 min at 37°C, prior to harvesting for immunoblot. To assess the DDR in the γH2AX knockout, cells were treated with 5 μM of bleomycin for 5 min before assessing by western blot.

Lentivirus production

To generate lentivirus expressing Rad51 or XLF shRNA, 1 μg/ml of pLKO.1 plasmid expressing Rad51 or XLF shRNA was co-transfected with 300 ng of pCMV-VSV-G, and 800 ng of psPAX2 in 2×10^6 293T cells in a 6-well plate using lipofectamine 3000, as described above. The sequences of Rad51 and XLF shRNA are shown in Supplementary Table S1. The culture medium was replenished with 4ml of fresh medium at 24 h post transfection, and cultured for another 48 h to allow lentivirus production. Lentivirus in the supernatant was collected after filtering with 0.45 μm filter.

KSHV and HSV

rKSHV.219 virus was induced from iSLK.219 cells (33). Cells were induced with 1 μg/ml doxycycline, 20 ng/ml tetradecanoyl phorbol acetate (TPA) and 1 mM sodium butyrate (NaB) for 16 h to induce Rta expression and activate the virus lytic cycle. Cells were subsequently maintained in culture media without TPA and NaB for an additional 4 days. The virus containing supernatant was harvested, and collected by ultracentrifugation at 25 000g for 4 h. The KSHV pellet was then suspended in a small volume of fresh DMEM medium containing 10% BGS and titrated by infecting 293T cells and assessing numbers of GFP positive cells (GFP expressed from the recombinant viral genome) by flow cytometry to determine infectious units. HSV-1 n212 stocks were kindly provided by David Knipe lab at Harvard Medical School (34)53 and titers determined.

Viral infection

For KSHV infection in 293T cells, $\sim 1 \times 10^6$ cells plated per well in 12-well plates, resulting in ∼70–80% confluence, and were infected with virus diluted in DMEM culture medium

containing 10% BGS at the indicated MOI. After 1–2 h of spinoculation by centrifugation at 3000 rpm × 1 hour at room temperature, cells were incubated at 37°C for the indicated time. For KSHV infection in SLK and HDMVEC cells, 0.2×10^6 cells were plated per well in 12-well plates, resulting in ∼70–80% confluence, and were infected at the indicated MOI. After spinoculation by centrifugation at 3000 rpm × 1 hour at room temperature, cells were incubated at 37°C for the indicated time. For KSHV infection of BJAB cells, 1×10^6 cells in 1 ml of RPMI culture medium containing 10% BGS per well in 12 -well plates were infected with KSHV at the indicated MOI. After 1 h of spinoculation by centrifugation at 3000 rpm × 1 h at room temperature, cells were incubated at 37°C for the indicated times. To assess KSHV lytic replication in 293T, SLK and HDMVEC cells, sodium phosphonoacetate (PAA) was added to the medium at 300 μg/ml at the time of infection and maintained in the culture medium to inhibit viral lytic DNA synthesis until cells were harvested at 24 hpi. KSHV infectious units were determined by infection of 293T cells followed by flow cytometry at 24 hpi to assess for recombinant viral GFP expression.

For HSV infection, $\sim 1 \times 10^6$ 293T cells were plated per well in 12-well plates, resulting in ∼70–80% confluence, and were infected with HSV-1 n212 at MOI ∼1 in 300 μl DMEM culture medium containing 2% BGS. The cells were incubated with virus inoculum for 1 h at 37°C with gentle agitation by tilting plates every 15 min. The inoculum was then removed by aspiration and replaced with 1 ml of fresh DMEM culture medium containing 10% BGS and 15 μg/ml gentamicin. To inhibit viral lytic DNA synthesis, PAA was included in the medium at 300 μg/ml from the time of initial infection until cells were harvested at 6 hpi.

ATM and DNAPK inhibitors

ATM kinase inhibitor KU-55933 (Catalog No.S1092, Selleckchem) and DNAPK inhibitor KU-57788 (Catalog No. S2638, Selleckchem) at concentrations ranging from 5 to 20 μM were incubated with SLK cells beginning 2 h prior to KSHV infection. 0.1% DMSO was used as a control. At 15 μM KU-55933 and/or KU-57788 or lower concentrations, SLK cells remained viable as assayed by trypan blue, and grew at a normal growth rate for at least 48 h incubation, while at higher concentrations, cells began to exhibit signs of toxicity. Similarly, HDMVEC cells retained normal growth and viability as assayed by trypan blue at 15 μM KU-55933 and/or KU-57788 for at least 24 h.

SDS-PAGE and western blotting

Proteins were resolved by SDS-PAGE, and transferred to nitrocellulose membranes for western blot. Membranes were incubated with primary antibody in PBS containing 0.05% Tween (PBST) at 4°C overnight followed by incubation with secondary antibody in PBST at room temperature for 1 h. The following antibodies were used at the indicated dilutions: anti-Flag (1804, Sigma-Aldrich, 1/5000), anti-H2AX (A300-082A, Bethyl Laboratories, 1/5000), anti-γH2AX (05–636, Millipore, 1/5000), anti-ATM (A300-136A,Bethyl Laboratories, 1/2000), anti-DNAPK (A303-967A, Bethyl Laboratories, 1/5000), anti-tubulin (66031-1-lg, Proteintech, 1/5000), anti-P-Chk2 (Thr68) (2197P, Cell Signaling Technology, 1/5000), anti-P-p53 (Ser15) (9286P, Cell Signaling Technology, 1/5000), anti-P-p95/NBS1 (Ser343) (3001P, 9286P, Cell Signaling Technology, 1/5000), anti-γH2AX (Ser139) (05–636, Millipore, 1/5000), anti-Rad51(8875S, Cell Signaling Technology, 1/5000), anti-Chk2 (2662S, Cell Signaling Technology, 1/1000), anti-p53 (sc-126, Santa Cruz Biotechnology, 1/1000), anti-p95/NBS1 (14956S, Cell Signaling Technology, 1/5000), anti-H2AX (A300-082A, Bethyl Laboratories, 1/5000 and anti-XLF (2854S, Cell Signaling Technology, 1/3000). Secondary antibodies used were goat anti-mouse IgG HRP (1030-05, Southern Biotech, 1/5000), goat anti-rabbit Ig HRP (4010–05, Southern Biotech, 1/5000), and bovine anti-goat IgG HRP (805-035-180, Jackson ImmunoResearch, 1/5000h).

Gardella gel and southern blot analysis

Infected cells were assessed by Gardella gel (35) after loading into agarose gel wells containing sodium dodecyl sulfate and DNase-free pronase protease (53702, Millipore). Following start of the gel run in Tris borate-EDTA buffer, cell lysis occurs. Gels were run overnight at 110 V at 4°C, and the following day, DNA transferred to a nylon membrane. KSHV DNA was detected using ^{32}P-labeled KSHV TR probe. HSV DNA was detected using ^{32}P-labeled HSV probe. Probe was generated with Prime-It II random primer Labeling Kit (300385, Agilent Technologies) following the manufacturer's instructions. ImageJ was used to quantify the intensity of the bands on Gardella gels. Intensity of the slower migrating, band, from circular DNA, was then divided by the sum of the intensities of the circular and linear bands for each lane. Fold change circularization was determined by relative circularization compared to WT or DMSO control for each Gardella gel. These values were then averaged for each set of experiments, and standard deviation determined.

Cell outgrowth and KSHV latency establishment assays

For KSHV latency establishment in BJAB cells, 3×10^6 cells per well in 3 ml of RPMI culture medium containing 10% BGS in 6-well plates, were infected with KSHV at MOI ∼20. After 1 h of spinoculation by centrifugation at 3000 rpm x 1 h at room temperature, cells and virus were maintained at 37°C. At 48 h post infection, flow cytometry was used to determine the percentage of GFP positive cells. 1000 GFP expressing cells (expressed by the recombinant virus) (as assessed by flow cytometry) were seeded per microtiter well, and placed under puromycin selection with 1 μg/ml, for which the virus encodes resistance. After 3 weeks of selection, the number of wells with puromycin resistant outgrowth was counted and divided by the total number of seeded GFP positive cells to calculate the efficiency of latency establishment.

For 293T cells, following infection at MOI ∼0.3, 1000 total cells from each infection were seeded in 150 mm tissue culture plates at 24 hpi and maintained in DMEM medium containing 1 μg/ml of puromycin. Mock infected cells were similarly seeded in the absence of puromycin. Due to the deficient growth of the double KO ATM/DNAPKcs cells, 2500 or 4000 cells were seeded for these cells (Supplementary Figure S4C). For Figure 1C, following infection at MOI ∼3, the total number of seeded cells was adjusted to contain 1000 GFP positive cells (as determined by flow cytometry). Following 3 weeks of puromycin selection, colonies were fixed in 2% formaldehyde for 1 hour, then washed with water. Plates were scanned into tiff files and processed with ImageJ to count

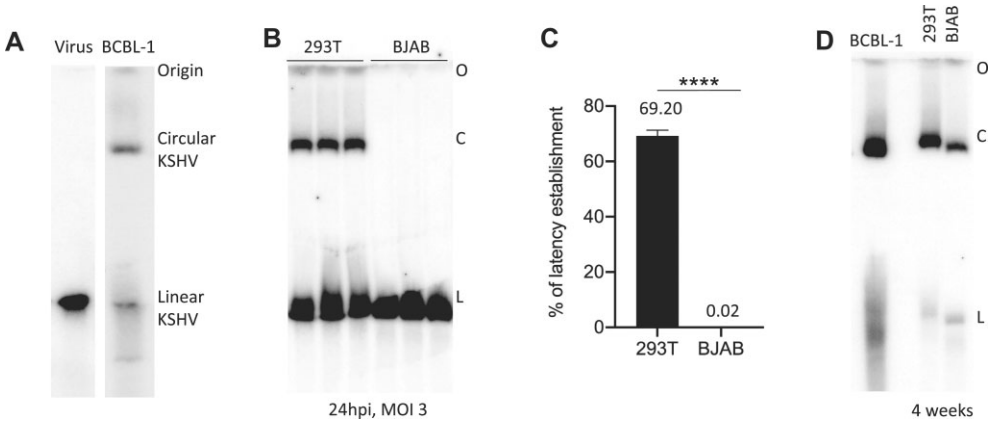

Figure 1. KSHV circularization and latency establishment are highly efficient in 293T cells, but deficient in BJAB B lymphoma cells. (**A**) Gardella gels of 0.5×10^6 rKSHV.219 infectious units or 1×10^6 BCBL1 PEL cells. Virions contain linear genomes, while BCBL1 cells contain circular, episomal KSHV genomes in latently infected cells, and linear DNA in a small subset of cells undergoing lytic replication. (**B**) Gardella gel containing rKSHV.219 infected 293T or BJAB cells at 24 hpi. Each lane contains an independent infection. (**C**) Efficiency of latency establishment in 293T or BJAB cells. Means are from three independent experiments. For 293T cells, outgrowth of 672, 714 and 690 colonies occurred per experimental plate, and for BJAB cells, 15,18, and 14 wells were positive per experimental plate. Standard deviation is shown. $^{****}P < 0.0001$ by unpaired t test. (**D**) Gardella gel of BCBL1 PEL cells, or rKSHV.219 infected 293T or BJAB cells after 4 weeks outgrowth (cells from experiment in Panel (C). 1×10^6 cells were loaded per well. O, gel origin; C, circular, episomal genomes; L, linear genomes.

colonies. Puromycin resistant cell outgrowth colony number was divided by the colony number of infected cells in the absence of selection for each cell line to account for cell growth differences. Ratios were compared to that of WT cells to determine fold change in KSHV latency establishment. At least three replicates were performed for the WT and each knockout cell line.

Flow cytometry

To determine the linear range of GFP expression, 0.2, 0.4, 0.6 or 1 μg of GFP expression plasmid were each transfected into BJAB or 293T cells, using Neon Transfection or lipofectamine 3000 respectively. At 24 h, the cells were analyzed by flow cytometry to determine the percentage of GFP positive cells in each transfection. The percentage of GFP positive cells was then plotted against GFP plasmid dosage to determine the linear range for GFP expression for each cell type (Supplementary Figure S6). To assess the efficiency of HR and NHEJ reporter DNA circularization, 0.4 μg of I-SceI linearized HR or NHEJ reporter DNA was co-transfected with 0.1 μg of DsRed2-C1 plasmid (which expresses DsRed2, a protein derived from red fluorescent protein (RFP), hereafter referred to as RFP) into 293T cells using lipofectamine 3000. The I-SceI digested linear plasmid was purified with NucleoSpin Plasmid Mini Kit (740588, Macherey-Nagel) prior to transfection. Twenty-four hours later, GFP and RFP expressing cells were resuspended in FACS buffer (1% BGS in PBS) and analyzed by flow cytometry (BD FACSCalibur). RFP expression was used to determine transfection efficiency and the ratio of GFP expressing cells to RFP expressing cells used to determine the efficiency of plasmid circularization. The GFP/RFP ratios were each divided by the average of results from WT cell transfections to determine fold change in reporter DNA circularization. Three replicates were performed for WT cells. Two independent ATM knockout, DNAPKcs knockout or ATM/DNAPKcs double knockout cell lines were analyzed, and each was repeated twice, with a total of 4 replicates for each gene knockout analyzed. To test the efficiency of HR and NHEJ reporter DNA circularization in BJAB cells, 0.8 μg of I-SceI linearized HR or NHEJ reporter DNA was each co-transfected with 0.2 μg of DsRed2-C1 plasmid into BJAB cells using the Neon Transfection System. Twenty-four hours post transfection, the efficiency of HR or NHEJ DNA circularization in BJAB cells was calculated by the ratio of GFP expressing cells to RFP expressing cells. The efficiency of reporter DNA circularization in 293T and BJAB cells was compared to calculate the fold change of reporter DNA circularization between different cell types. Three replicates were performed for each reporter in each cell type.

Fluorescence microscopy

GFP expressing cell images were captured using a Zeiss Axiovert 200 fluorescent microscope with Axiovision AC imaging software (Zeiss) at 100 × magnification.

Quantification and statistical analysis

Statistical calculations were performed using GraphPad Prism 7 (GraphPad Software Inc.). Specific information for each figure is provided in the figure legends.

Results

KSHV circularization and latency establishment efficiency differs between cell types

We used Gardella gels (35) to assess genome circularization following primary infection of rKSHV.219 (36), a recombinant KSHV that constitutively expresses GFP. (36) In Gardella gels, virions or live cells are loaded in gel wells and are lysed *in situ* at the start of the gel run. Viral genomic DNA (as large as 200 kb) migrates into the gel, while host chromosomal DNA remains at the origin. Gardella gels distinguish between linear and covalently closed, circular, DNA. As expected, rKSHV.219 virions contained only linear DNA, while naturally infected BCBL1 PEL cells contain both

linear and circular, episomal, KSHV DNA (Figure 1A). The episomal DNA is primarily from latently infected cells, while the linear DNA in BCBL1 cells is from a small subset of cells undergoing lytic replication. Episomal KSHV DNA has a decreased mobility compared to linear genomic DNA.

We investigated the efficiency of genome circularization in 293T cells and BJAB B lymphoma cells following rKSHV.219 infection at multiplicity of infection (MOI) ∼3. At 24 h post infection (hpi), circular rKSHV.219 DNA was easily detected in 293T cells, but was not detectable in BJAB cells (Figure 1B). We considered the possibility that the undetectable circular DNA might be due to low efficiency of infection in BJAB cells. The recombinant rKSHV.219 used was generated from iSLK.219 cells, and encodes the green fluorescent protein (GFP) under the control of a constitutive promoter. Following infection at MOI ∼0.5 in 293T cells, and MOI ∼20 in BJAB cells, ∼30% of cells expressed GFP (Supplementary Figure S1A). Despite the similar numbers of cells with virus infection as indicated by GFP expression, Gardella gel analysis demonstrated that rKSHV.219 genome circularization was easily detectable in 293T cells, but not in BJAB cells (Supplementary Figure S1B). Therefore, genome circularization efficiently occurs in 293T cells, but not in BJAB cells.

Since linear KSHV genomes must circularize to establish latent infection, deficient genome circularization is expected to lead to deficient latency establishment. We therefore assessed the outgrowth efficiency of latently infected cells following infection of 293T or BJAB cells. In addition to encoding GFP, rKSHV.219 virus constitutively expresses puromycin N-acetyl-transferase, which engenders puromycin resistance, allowing puromycin selection of latently infected cell outgrowth. Assessing the outgrowth of rKSHV.219 latently infected cells allows determination of latency establishment efficiency. For 293T cells, 1000 virus infected 293T cells, as assessed by GFP expression, were seeded into 15 cm dishes, and placed under puromycin selection at 24 hpi. After 3 weeks of selection, the number of puromycin resistant 293T cell colonies was determined. For BJAB cells, at 48 hpi, 1000 virus infected cells, similarly assessed by GFP expression, were seeded per well in 96 well microtiter plates. Following 3 weeks of selection, the number of wells with puromycin resistant outgrowth was determined. Altogether, puromycin resistant 293T cell outgrowth occurred in ∼70% of infected cells, whereas BJAB outgrowth occurred in only ∼0.02% of infected cells (Figure 1C), a ∼3500-fold difference. This difference, several orders of magnitude, reflected the difference in 293T and BJAB circularization efficiencies, for which circularization was easily detectable in 293T cells, but undetectable in BJAB cells (Figure 1B).

Since a small percentage of BJAB infected cells grew out as latently infected, puromycin resistant cell lines, we assessed for rKSHV.219 circularization in these cells, since all latently infected cell lines are expected to contain circular viral forms, and which are strongly selected for in this assay. Following four weeks of puromycin resistant cell outgrowth, 293T or BJAB cells were assessed by Gardella gel analysis. As expected, 293T cells contained circular, episomal, and linear KSHV DNA (from a small subset of cells undergoing lytic replication) (Figure 1D). BJAB cells also contained circular and linear KSHV DNA. The circular DNA is due to episomes, while linear DNA is from a small subset of cells undergoing lytic infection. (37–39) These results indicate circularization of the KSHV genome occurs in BJAB cells, but at very low efficiency, and can be selected for in latency outgrowth assays. These data also provide evidence in support of a requirement for circularization for virus persistence in a latent state.

KSHV genome circularization occurs rapidly, and is independent of viral protein expression

We assessed the kinetics of viral genome circularization. Gardella gels were performed at 15–30 min intervals starting 60 min following infection by spinoculation of 293T cells at MOI 3. Faint, circular KSHV DNA signal was observed as of 160 min pi, and signal increased at 180 min pi (Figure 2A).

Following infection, HSV circularization does not require *de novo* protein synthesis. (26,40,41) Since the rapid KSHV genome circularization following infection suggested that viral gene expression was also not necessary for KSHV episome formation, we investigated this possibility. Cells were infected with or without incubation with cycloheximide to inhibit protein synthesis. GFP expression was easily detectable following infection in the absence of cycloheximide, but was absent following infection in the presence of cycloheximide (Figure 2B), indicating efficient inhibition of viral gene expression. Gardella gel analysis demonstrated viral genome circularization at equivalent levels in both the presence and absence of cycloheximide (Figure 2B). Therefore, *de novo* viral protein synthesis is not required for KSHV genome circularization. As KSHV virions contain tegument proteins, it remains possible that these protein(s) could be involved in genome circularization.

Loss of ATM and DNAPKcs reduces the DDR following bleomycin or KSHV infection

Since viral protein expression is dispensable for circularization, KSHV may utilize cellular machinery for genome circularization. The free DNA ends of the linear viral genome mimic DNA at sites of DSBs, and therefore may be ligated by DSB repair mechanisms. We investigated the roles of ATM or DNAPK, the two apical PIKKs that play key roles in DSB repair, in circularizing the KSHV genome. ATM or DNAPKcs were each targeted by CRISPR/Cas9 for knockout (KO) in 293T cells (Figure 3A). In addition, cells knocked out for both ATM and DNAPKcs were generated (Figure 3A).

We investigated the effect loss of ATM or DNAPKcs, or double KO of ATM and DNAPKcs, on the DDR. As expected, incubation with the DNA damaging agent bleomycin, a DDR occurred in WT 293T cells, as evidenced by phosphorylation of CHK2, NBS1, p53 and H2AX (Figure 3A). Loss of ATM or DNAPKcs did not alter CHK2 or NBS1 phosphorylation. However, loss of both ATM and DNAPKcs resulted in absence of increase in CHK2 or NBS1 phosphorylation (Figure 3A). In contrast to results with CHK2 or NBS1, following bleomycin, p53 phosphorylation was reduced in ATM or DNAPKcs KO cells and further reduced in ATM/DNAPKcs double KO cells (Figure 3A). ATM or DNAPKcs KO also led to low levels of baseline p53 phosphorylation in the absence of bleomycin, and ATM/DNAPKcs double KO cells had even higher levels (Figure 3A, bottom panel). Phosphorylated H2AX (γH2AX) levels were also affected by ATM and/or DNAPKcs KO. Following bleomycin, γH2AX was modestly reduced in ATM

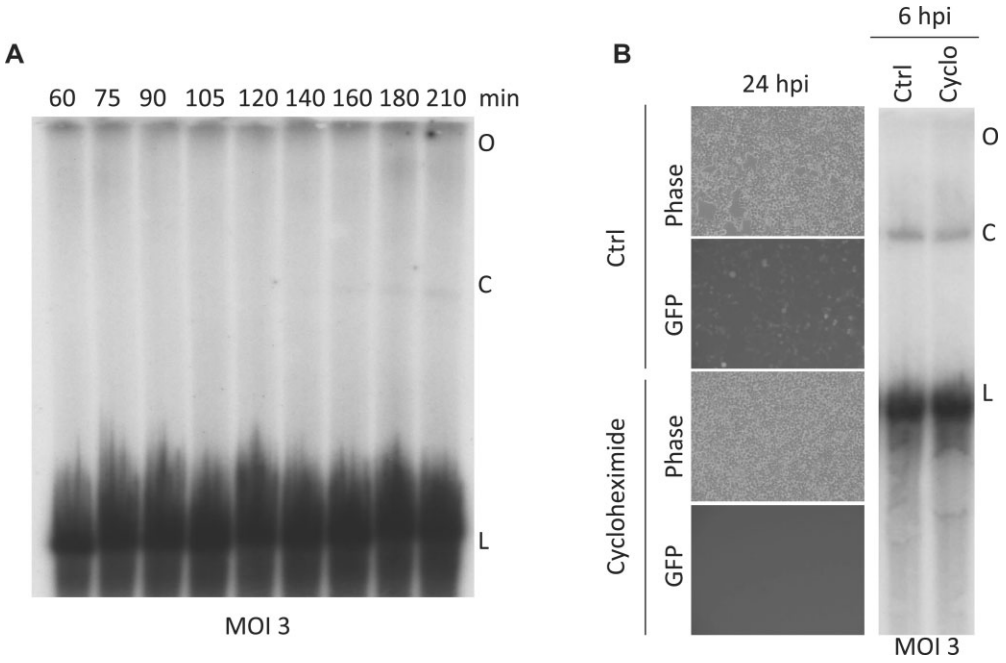

Figure 2. KSHV rapidly circularizes and viral protein expression is dispensable for circularization. (**A**) Gardella gel of rKSHV.219 infected 293T cells at different time points pi. For each lane, ~0.6 × 10^6 cells were initially infected by spinoculation for 1 h at MOI ~3. (**B**) ~0.6 × 10^6 cells were infected by spinoculation for 2 h at MOI ~3 in the presence or absence of 10 μg/ml cycloheximide and cells imaged by phase microscopy at 24 hpi for GFP (expressed from the recombinant viral genome) fluorescence. Gardella gel was performed at 6 hpi. O, gel origin; C, circular, episomal genomes; L, linear genomes.

KO cells, substantially reduced in DNAPKcs KO cells, and nearly absent in double ATM/DNAPKcs KO cells (Figure 3A). Therefore, following bleomycin, loss of ATM or DNAPKcs reduces the DDR and loss of both ATM and DNAPKcs nearly abolishes the DDR as assessed by phosphorylation of these DDR related factors.

We also investigated the DDR following rKSHV.219 infection at 3 hpi, when circularization first begins to occur (Supplementary Figure S2A), or 24 hpi, when circularization is robust (Figure 3B). rKSHV.219 infection at MOI 3 induced a DDR, as indicated by γH2AX signal in WT 293T cells at 3 hpi, which increased at 24 hpi (Figure 3B). Knockout of ATM led to reduced γH2AX level at 3 or 24 hpi, and no γH2AX induction occurred following infection of either DNAPKcs KO cells or ATM/DNAPKcs double KO cells. rKSHV.219 infection at MOI 3 did not induce detectable phosphorylation of CHK2, NBS1 or p53 at 3 or 24 hpi in WT or KO cells (Figure 3B, Supplementary Figure S2A). Therefore, at MOI 3, rKSHV.219 induces a DDR as evidenced by γH2AX in WT 293T cells. This response is reduced in ATM KO cells, and absent in DNAPKcs KO or ATM/DNAPKcs double KO cells.

KSHV infects epithelial cells *in vivo*, and KS spindle cells are felt to be of endothelial origin.(42,43) Therefore, in addition to 293T cells, we investigated the DDR induced by rKSHV.219 infection in SLK epithelial cells or primary human dermal microvascular endothelial cells (HDMVECs). As expected, bleomycin induced robust phosphorylation of CHK2, NBS1 and γH2AX in either SLK or HDMVEC cells (Figures 3C, D, Supplementary Figure S2C, D). Unexpectedly, bleomycin did not induce detectable p53 phosphorylation, possibly due to the low p53 levels in these cells compared with 293T cells (Supplementary Figure S2E, F). Since viral genome circularization was detectable by Gardella gel at 24 hpi following rKSHV.219 infection of SLK cells at MOI 3 (Figure 3C, upper panel, first lane) or at 12 hpi following rKSHV.219 infection of HDMVEC cells at MOI 10 (Figure 3D, upper panel, first lane), we assessed the DDR at these time points under these conditions. Similar to 293T cells, no detectable phosphorylation of CHK2, NBS1 or p53, was observed. However, in contrast to 293T cells no γH2AX phosphorylation was observed either (Figure 3C, D, DMSO lanes).

Since a previous report described KSHV infection of HDMVEC cells at MOI 30 induced detectable γH2AX and CHK2 phosphorylation that reached maximal levels at 3 hpi (19), we assessed the DDR following infection at MOI 30 in 293T, SLK and HDMVEC cells at 3 hpi. For 293T cells, rKSHV.219 infection at MOI 30 induced a similar γH2AX signal as that observed following infection at MOI 3.0 at 3 hpi (compare Supplementary Figures S2A (WT lane) with S2B (DMSO lane), and similarly did not result in CHK2, NBS1, or p53 phosphorylation (Supplementary Figure S2B). As with the ATM and DNAPKcs knockouts (Supplementary Figure S2A), incubation with ATM inhibitor KU55933 resulted in reduced 293T γH2AX signal, and DNAPK inhibitor KU57788, or combined ATM/DNAPK inhibitors, prevented γH2AX activation (Supplementary Figure S2B). Similar to 293T cells, SLK and HDMVEC cells exhibited γH2AX signal at 3hpi, which was reduced by incubation of ATM inhibitor and abolished by incubation with DNAPK or combined ATM/DNAPK inhibitors (Supplementary Figure S2C, D). Also similar to 293T cells, no CHK2, NBS1 or p53 phosphorylation was detected (Supplementary Figure S2C, D). It is possible that the absence of CHK2 phosphorylation in DMVECs at 3 hpi compared to prior work (19) is related to host donor differences of these primary cells. Therefore, the DDR responses following rKSHV.219 infection were similar for 293T, SLK, and DMVEC cells at 3 hpi when circularization

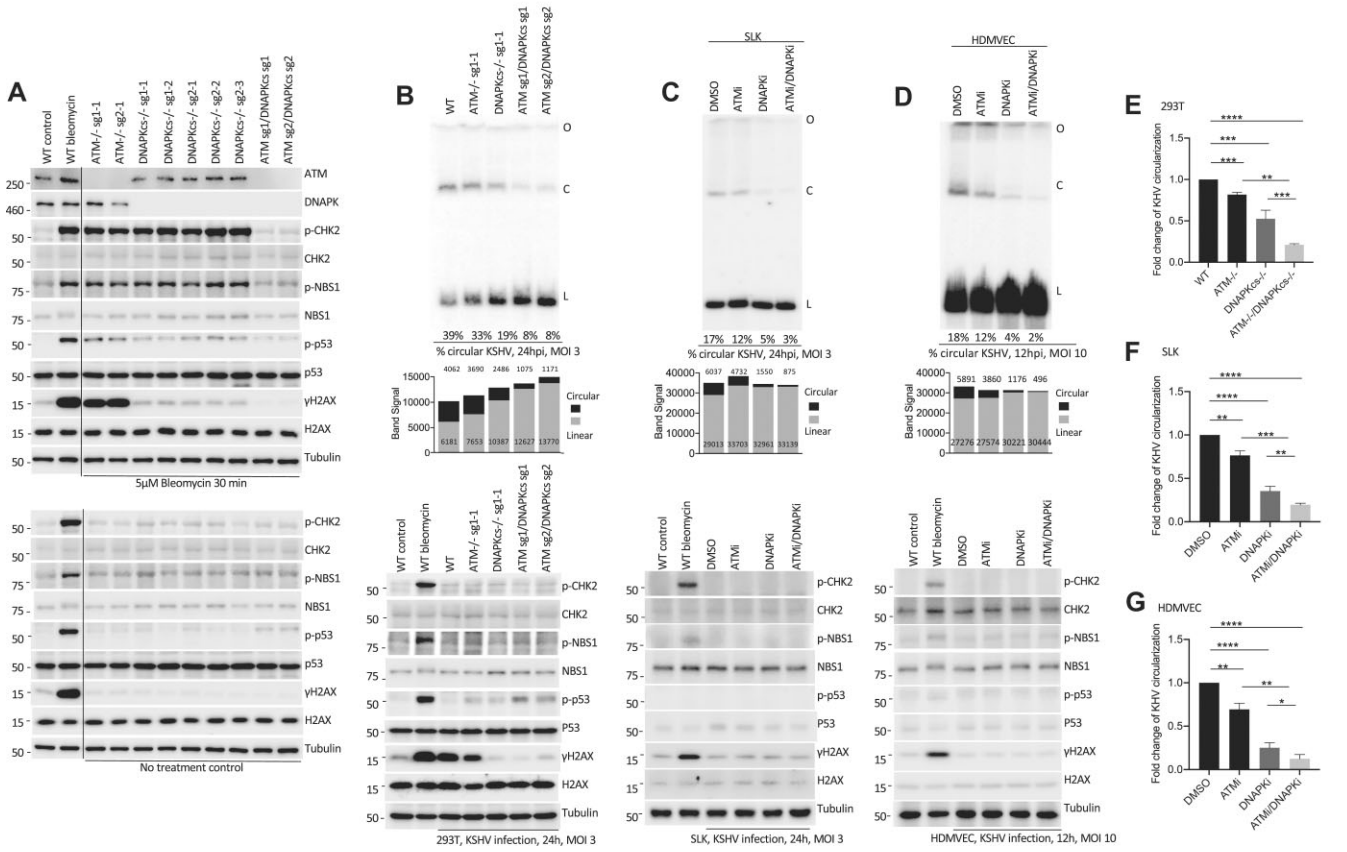

Figure 3. ATM and DNAPKcs exert roles in the DDR and KSHV circularization. (**A**) Immunoblot of ATM, DNAPKcs, CHK2, phosphorylated CHK2, NBS1, phosphorylated NBS1, p53, phosphorylated p53, H2AX, γH2AX in WT or ATM or DNAPKcs CRISPR/Cas9 targeted cells with or without incubation with bleomycin. Size markers (kDa) at left. (**B**) Upper panel shows Gardella gel of rKSHV.219 infected WT 293T cells, ATM-/-, DNAPKcs -/-, or ATM/DNAPKcs double knockout cells. Results representative of at least three independent experiments. Middle panel: Gardella gel circular and linear band quantitation. Bottom panel: immunoblot of phosphorylated CHK2, CHK2, NBS1, phosphorylated NBS1, p53, phosphorylated p53, H2AX or γH2AX in cells with or without rKSHV.219 infection. (**C**) Upper panel shows Gardella gel following rKSHV.219 infection of SLK cells with incubation with DMSO, 15 μM KU55933 ATM inhibitor, 15 μM KU57788 DNA-PK inhibitor, or both. Results representative of three independent experiments. Middle panel: Gardella gel circular and linear band quantitation. Bottom panel: immunoblot of phosphorylated CHK2, CHK2, NBS1, phosphorylated NBS1, phosphorylated p53, p53, γH2AX or H2AX in cells with or without rKSHV.219 infection. (**D**) Upper panel: Gardella gel following rKSHV.219 infection of HDMVEC cells with incubation with DMSO, 15 μM KU55933 ATM inhibitor, 15 μM KU57788 DNA-PK inhibitor, or both. Results representative of three independent experiments. Middle panel: Gardella gel circular and linear band quantitation. Bottom panel: immunoblot of phosphorylated CHK2, CHK2, phosphorylated NBS1, NBS1, phosphorylated p53, p53, γH2AX, or H2AX or in cells with or without rKSHV.219 infection. (B–D) Percentage of KSHV genome that is circular is indicated. O, gel origin; C, circular, episomal genomes; L, linear genomes. Bleomycin treated cells are a positive control for activation of DDR markers. (**E**) Fold change circularization following rKSHV.219 infection of WT 293T cells compared to ATM-/-, DNAPKcs-/- or ATM/DNAPKcs double knockout cells. Primary data shown in panel B, Supplementary Figure S2G-I. (F, G) Fold change circularization following rKSHV.219 infection of (**F**) SLK or (**G**) HDMVEC cells and incubation with 15 μM KU55933 ATM inhibitor, 15 μM KU57788 DNA-PK inhibitor, or both compared with DMSO control. Primary data shown in panels C, D, Supplementary Figure S2J, K. (E–G) Results from three independent experiments. Standard deviations are shown. * $P < 0.05$; ** $P < 0.01$; *** $P < 0.001$; **** $P < 0.0001$ by unpaired *t* test.

begins, and exhibited only γH2AX signal. Loss of ATM activity reduced, and loss of DNAPK or both ATM/DNAPK activity abolished a detectable DDR for these cells.

ATM and DNAPKcs are critical for KSHV circularization and latency establishment

We assessed KSHV circularization efficiency by Gardella gel in WT 293T, ATM or DNAPKcs knockout cells, or in ATM/DNAPKcs double KO cells. At 24 hpi, circularization was slightly reduced in ATM KO versus WT as evidenced by ∼10% less band signal of the circular form, and ∼25% increased linear genomic band signal was also observed (Figure 3B, Supplementary Figure S2G, H, upper panels with quantitation beneath). DNAPKcs KO cells had a moderate circularization deficit (∼40% less band signal compared to WT), and increased linear genomic signal was also present (Figure 3B, Supplementary Figure S2G, I). Absence of both ATM and DNAPKcs resulted in severe circularization deficiency (∼75% less band signal compared to WT) (Figure 3B, Supplementary Figure S2G), that was synergistic compared to KO of either gene alone, and further increased linear genomic signal. As a result of the decreased circular genomes and increased linear genome, the percent of genome that was circularized fell with loss of DDR function (Figure 3B, E, Supplementary Figure S2G-I). Interestingly, the degree of increase in linear genomic signal cannot be fully accounted for by the deficiencies in levels of circularized genomes, suggesting degradation of some linear genomes may occur as genomes are circularized.

We also assessed the effect of ATM or DNAPKcs chemical inhibition on KSHV circularization following infection of

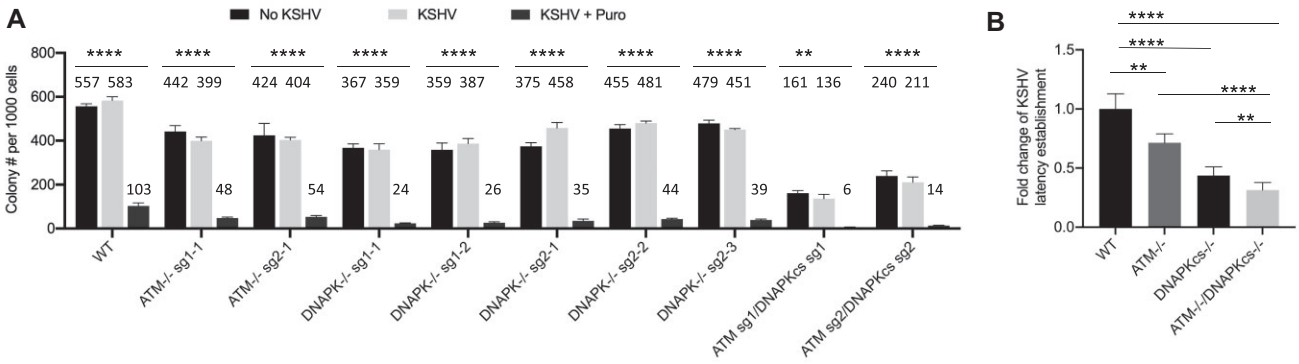

Figure 4. ATM and DNAPKcs are important for KSHV latency establishment. (**A**) Outgrowth of WT, ATM-/-, DNAPKcs-/- or ATM/DNAPKcs double KO cells with or without rKSHV.219 infection or puromycin selection. Data were collected 3 weeks pi. Means with standard deviation from three independent experiments are shown. In the absence of rKSHV.219 infection, there was no puromycin resistant colony outgrowth. ** $P < 0.01$; ****, $P < 0.0001$ by chi square. (**B**) Fold change of rKSHV.219 latency establishment compared to WT for ATM-/-, DNAPKcs-/- or ATM/DNAPKcs double KO cells. Primary data are from Supplementary Figure S3. Standard deviation is shown. ** $P < 0.01$; **** $P < 0.0001$ by unpaired t test.

SLK epithelial cells or primary HDMVEC endothelial cells. While inhibition of ATM with 15 μM KU55933 slightly reduced virus circularization (∼20% less SLK, or ∼35% less DMVEC circular band signal compared to DMSO), inhibition of DNA-PK with 15 μM KU57788 substantially reduced (∼35–75% less SLK, or ∼65–80% less DMVEC circular band signal compared to DMSO) circularization (Figure 3C, D, Supplementary Figure S2J, K), and simultaneous inhibition of ATM and DNA-PK nearly abolished circularization (Figure 3C, D, Supplementary Figure S2J, K). As a result, the circular fraction of viral genome progressively decreased with inhibition of ATM, DNA-PK, or simultaneous inhibition of both (Figure 3C, D, F, G, Supplementary Figure S2J, K). Similar to 293T cells, increased linear viral genomic signal was generally observed with increasing inhibition of circularization. This increased signal was not due to lytic replication since there was no reduction following incubation with PAA, which inhibits KSHV DNA polymerase (Supplementary Figure S2L). Therefore, this linear signal is from input viral DNA, which diminishes with increasing levels of circularization, similar to 293T cells.

Since linear KSHV must circularize to establish latency, we hypothesized deficiency in circularization following de novo infection would be associated with deficiency in latency establishment. We investigated the effect of knockout of ATM or DNAPKcs, or the effect of double knockout of both ATM and DNAPKcs, on viral latency. Since ATM and/or DNAPKcs deficiency potentially exert effects on cell growth, we also assessed outgrowth of uninfected cells to allow for correction of any growth deficiency. Colony outgrowth of uninfected cells after ∼2–3 weeks was modestly reduced for ATM or DNAPKcs KO cells, and further reduced in double KO ATM/DNAPKcs cells (Figure 4A, Supplementary Figure S3). The reductions in cell growth may be in part due to elevated baseline levels of phosphorylated p53 in the KO cells, which is highest in the ATM/DNAPKcs double KO cells (Figure 3A). rKSHV.219 infection in the absence of drug selection for infected cells, had no effect on outgrowth (Figure 4A, Supplementary Figure S3).

To assess KSHV latency establishment, we infected cells at MOI ∼0.3 to promote clonal infection, and determined puromycin resistant cell outgrowth at ∼2–3 weeks pi. To correct for reduced cell growth rates in the KO cell lines, puromycin resistant outgrowth was normalized to cell outgrowth in the absence of selection for each cell line (Figure 4A, B; Supplementary Figure S3). Results showed absence of ATM induced a latency establishment deficiency of ∼30%, KO of DNAPKcs resulted in a deficiency of greater than 50%, and double KO of ATM/DNAPKcs led to high level deficiency of ∼70% (Figure 4B). Remarkably, these deficiencies closely mirrored the reductions in circular band signal on Gardella gel analyses (∼10% for ATM KO, ∼40% for DNAPKcs KO, and ∼75% for ATM/DNAPKcs knockout) discussed above (Figures 3B, S2). Therefore, ATM and DNAPKcs have important roles in both viral genome circularization and latency establishment, and ATM/DNAPKcs double KO results in severe deficiency.

ATM and DNAPKcs catalytic activity exert roles in KSHV circularization and latency establishment

We asked if ATM or DNAPKcs catalytic activity exert roles in viral genome circularization. ATM containing the substitutions D2870A and N2875K (27) and DNAPKcs with a T3950D substitution (29) are catalytically inactive. Transient expression of WT ATM and DNAPKcs in ATM/DNAPKcs double knockout cells (Figure 5A) moderately increased genome circularization in these cells as evidenced by ∼50% increased circular band signal or fold change circularization (Figure 5B, C; Supplementary Figure S4A). Although circularization did not reach WT levels, this finding is likely attributable to the large sizes of ATM (∼350 kDa, 3056 amino acids) and DNAPKcs (∼469 kD, 4128 amino acids) and transient expression in only a subset of cells, while infection at MOI ∼3 is expected in nearly all cells. In fact, immunoblot demonstrated substantially lower levels of these proteins compared to WT levels (Supplementary Figure S4B). In direct contrast, expression of the catalytically inactive ATM and DNAPKcs mutants did not increase circularization.

Since transient expression of WT ATM and DNAPKcs in ATM/DNAPKcs double knockout cells modestly increased circularization, we assessed if latency established was also increased. To correct for reduced KO cell line growth rates, puromycin resistant outgrowth was normalized to cell outgrowth in the absence of drug selection, following expression of ATM and DNAPKcs, or the catalytic mutants (Figure 5D, E; Supplementary Figure S4C). Transient

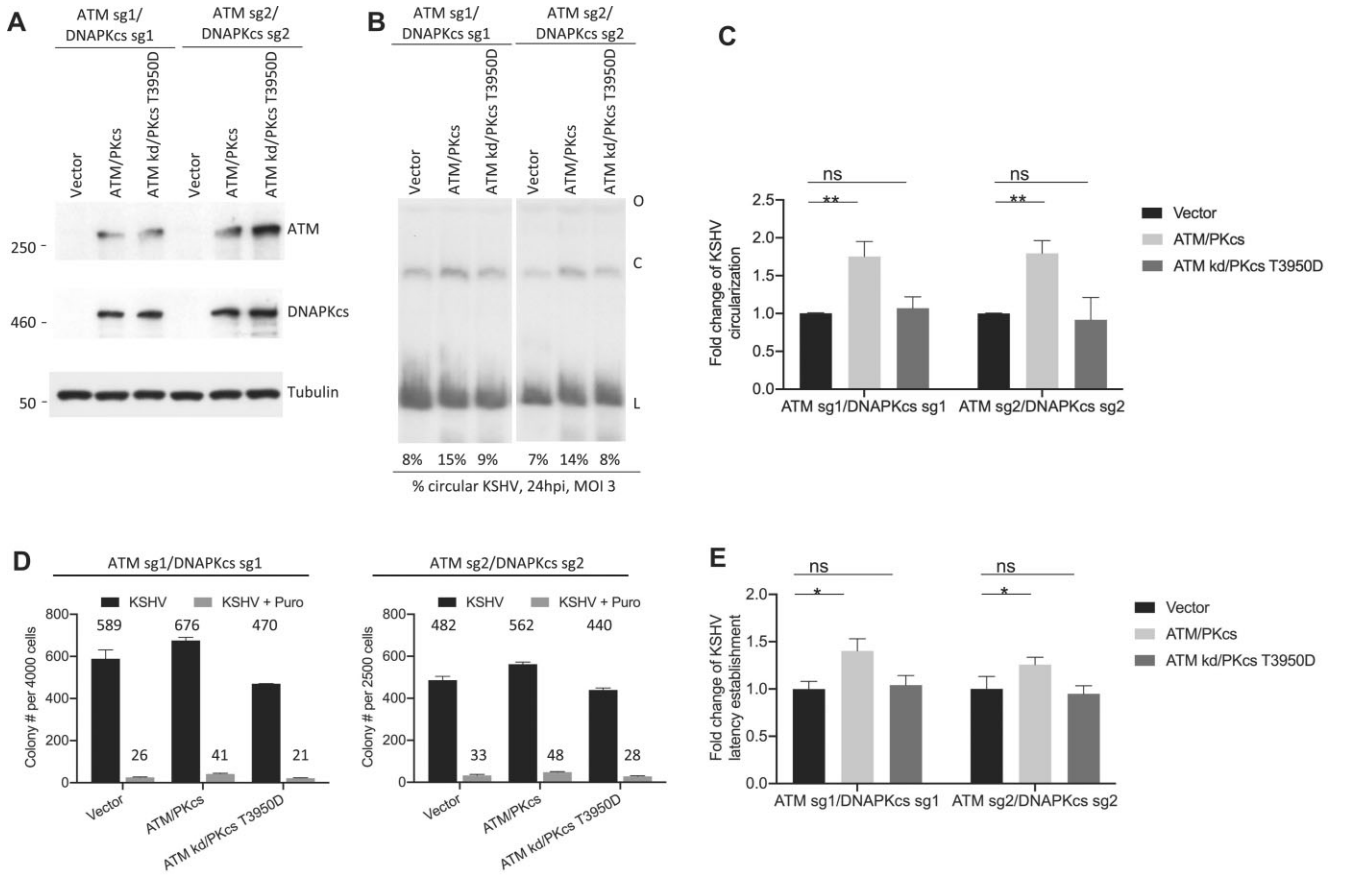

Figure 5. ATM and DNAPKcs catalytic activity exert roles in KSHV circularization and latency establishment. (**A**) Immunoblot of ATM/DNAPKcs double KO cells, with or without transient expression of ATM and DNAPKcs, or ATM kd and DNAPKcs T3950D catalytic mutants. Size markers (kDa) at left. (**B**). Gardella gel of ATM/DNAPKcs double KO cells with or without expression of WT or catalytic ATM and DNAPKcs mutants. Percentage of KSHV genome that is circular is indicated. Results representative of three independent experiments (shown in Supplementary Figure S4A). (**C**) Fold change KSHV genome circularization in ATM/DNAPKcs double KO cells for data in panel C and Supplementary Figure S4A. (**D**) Outgrowth of rKSHV.219 latently infected colonies after infection of ATM/DNAPKcs double KO cells, with or without transient expression of ATM and DNAPKcs, or ATM and DNAPKcs catalytic mutants, and with or without puromycin selection. Data were collected 3 weeks pi. Primary data in Supplementary Figure S4C. (**E**) Fold change of rKSHV.219 latency establishment of ATM/DNAPKcs double KO cells for data in panel D Standard deviation is shown for panels C, E. ns, $P > 0.05$; * $P < 0.05$, ** $P < 0.01$ by unpaired *t* test.

expression of WT ATM and DNAPKcs in the double knockout cells increased outgrowth of latently infected, puromycin resistant cells by up to ∼40% (Figure 5E), similar to the level of increased circularization observed on Gardella gel. In contrast, expression of the ATM and DNAPKcs catalytic mutants had no effect on viral latency establishment. Therefore, ATM and DNAPKcs catalytic activity are important for KSHV circularization and latency establishment.

γH2AX does not contribute to KSHV circularization, but has a role in latency establishment

Phosphorylation of histone H2AX to γH2AX at sites of DSBs is an important marker of DDR activation. KSHV infection, which induces a DDR, induced γH2AX at 24 hpi (Figure 3B). Previous work demonstrated that ATM and DNAPK function redundantly to phosphorylate H2AX (44). Since DNAPKcs KO had a greater effect than did ATM KO on both H2AX phosphorylation (Figure 3B), and viral circularization (Figure 3B) following infection, it raised the possibility that γH2AX might have a role in the circularization process.

To test the role of H2AX phosphorylation in viral circularization, we targeted C-terminal H2AX at the serine 130 position (^{130}SGGKKATQASQEY^{142}) using CRISPR/Cas9 to generate γH2AX-/- cells. H2AX serine 139, the phosphorylated amino acid in DDR activation, cannot be phosphorylated in these cells (Figure 6A). Following infection, Gardella gel analysis revealed that rKSHV.219 circularization in γH2AX-/- cells was similar to that in WT cells (Figure 6B; Supplementary Figure S5A). We also assessed latency establishment in γH2AX-/- cells. Despite the absence of effects on circularization, latently infected cell outgrowth was reduced about 50% in γH2AX-/- cells (Figure 6C, D; Supplementary Figure S5B). These results show that H2AX phosphorylation is not important for viral DNA circularization, but does have a role in KSHV latency establishment.

HR and NHEJ both contribute to KSHV circularization

We assessed the role of HR and NHEJ, two prominent cellular DSB repair mechanisms, (13) in virus circularization. HR utilizes a homologous stretch of DNA as a template to re-synthesize the damaged sequence at DSB sites while NHEJ re-ligates the broken DNA ends directly (Figure 7A). DNAPK, of which DNAPKcs is the catalytic subunit, has a central role

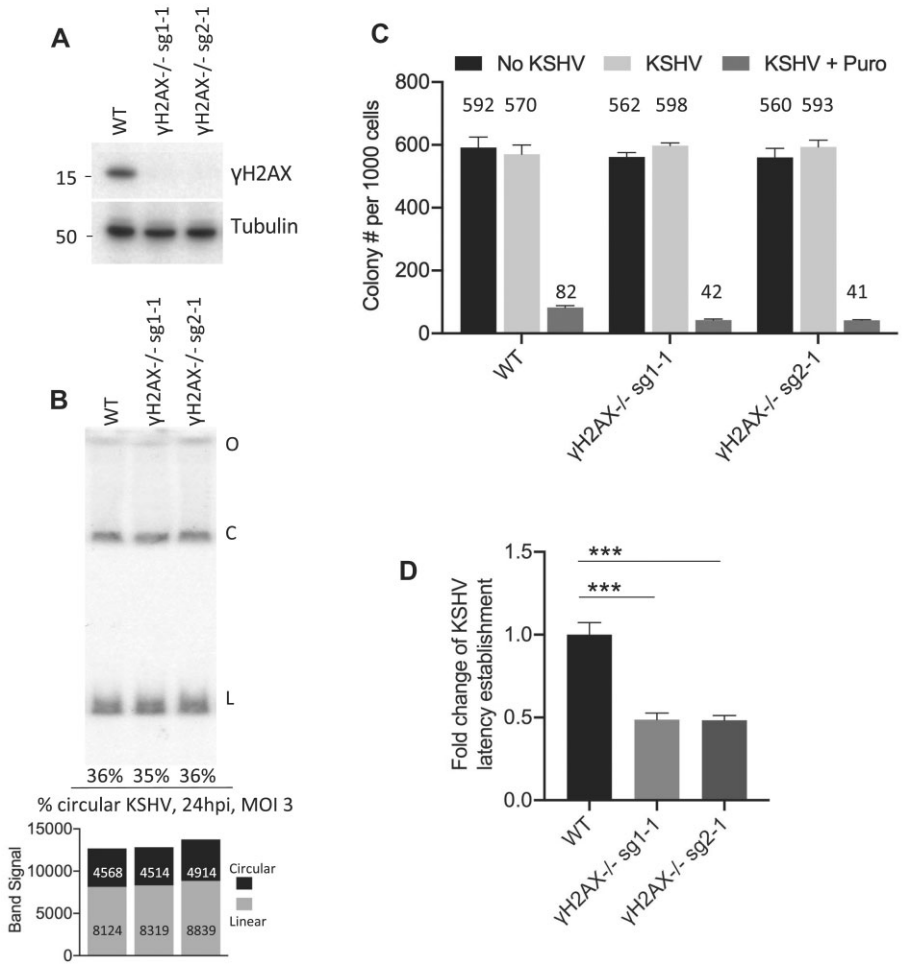

Figure 6. H2AX phosphorylation to γH2AX is dispensable for KSHV circularization, but has a role in latency establishment. (A) Immunoblot for γH2AX in WT or γH2AX-/- cells following incubation with bleomycin. (**B**) Gardella gel following rKSHV.219 infection of WT or γH2AX-/- cells. Results representative of two experiments. Circular and linear band signal, and percentage of KSHV genome that is circular is indicated. O, gel origin; C, circular, episomal genomes; L, linear genomes. (**C**) Outgrowth of WT or γH2AX-/- cells with or without rKSHV.219 infection or puromycin selection. Numbers indicate colony counts at 3 weeks pi. (**D**) Fold change of rKSHV.219 latency establishment following infection of WT or γH2AX-/- cells for data in panel C. Standard deviation is shown. *** $P < 0.001$ by unpaired t test.

in the NHEJ pathway. DNAPKcs interacts with Ku70 and Ku80 to form a synaptic complex at DNA termini to allow ligation (45). ATM promotes HR through phosphorylation of a number of DSB response proteins (46). However, ATM also phosphorylates key components of the NHEJ repair pathway, such as DNAPKcs and DNA polymerase lambda. (47,48) Therefore, while KO of DNAPKcs suggests NHEJ is important for virus circularization, the deficiency in circularization induced by KO of ATM could be due to its role in HR and/or NHEJ (Figure 7B). HR can potentially occur since the virus termini are within repetitive TR elements.

To address the roles of NHEJ or HR in virus circularization, we assessed these processes in ATM or DNAPKcs KO cells. We used reporter systems for these repair pathways which rely either on NHEJ or HR to circularize a linearized vector to allow GFP expression (Figure 7C). (32,49,50) We cotransfected an RFP expression vector with the reporter to normalize for transfection efficiency. In this system, the ratio of GFP to RFP expressing cells indicates NHEJ or HR efficiency. As expected, DNAPKcs knockout cells were highly (~80%) deficient for NHEJ (Figure 7D, Supplementary Figures S6, S7), but were not reduced for HR (Figure 7E, Supplementary Figures S6, S7). In fact, HR was higher in DNAPKcs knockout cells, which could be due to the increase in available template for HR, in the absence of NHEJ. In contrast, ATM knockout cells were reduced for both HR (by ~60%) and NHEJ (by ~75%) (Figure 7D, E, Supplementary Figure S7). Cells knocked out for both ATM and DNAPKcs were also severely (~85%) reduced for NHEJ, and had a similar reduction in HR as ATM knockout cells alone (Figure 7D, E, Supplementary Figure S7). Therefore, DNAPKcs knockout induces severe deficiency in NHEJ, while ATM KO induces deficiency in both HR and NHEJ. Since ATM knockout induces only a small effect in KSHV circularization, KSHV must largely compensate for the loss of ATM, such as through activation of other kinases.

Since the role of ATM is not specific to HR or NHEJ, we further assessed the role of HR by targeting Rad51. Rad51 is a key protein for HR, binding to single-strand DNA (ssDNA) generated following end resection at DSBs, and forms a nucleoprotein filament to mediate strand invasion, allowing HR to occur.(51) Since Rad51 is an essential gene, we targeted it by shRNA knockdown rather than knockout.

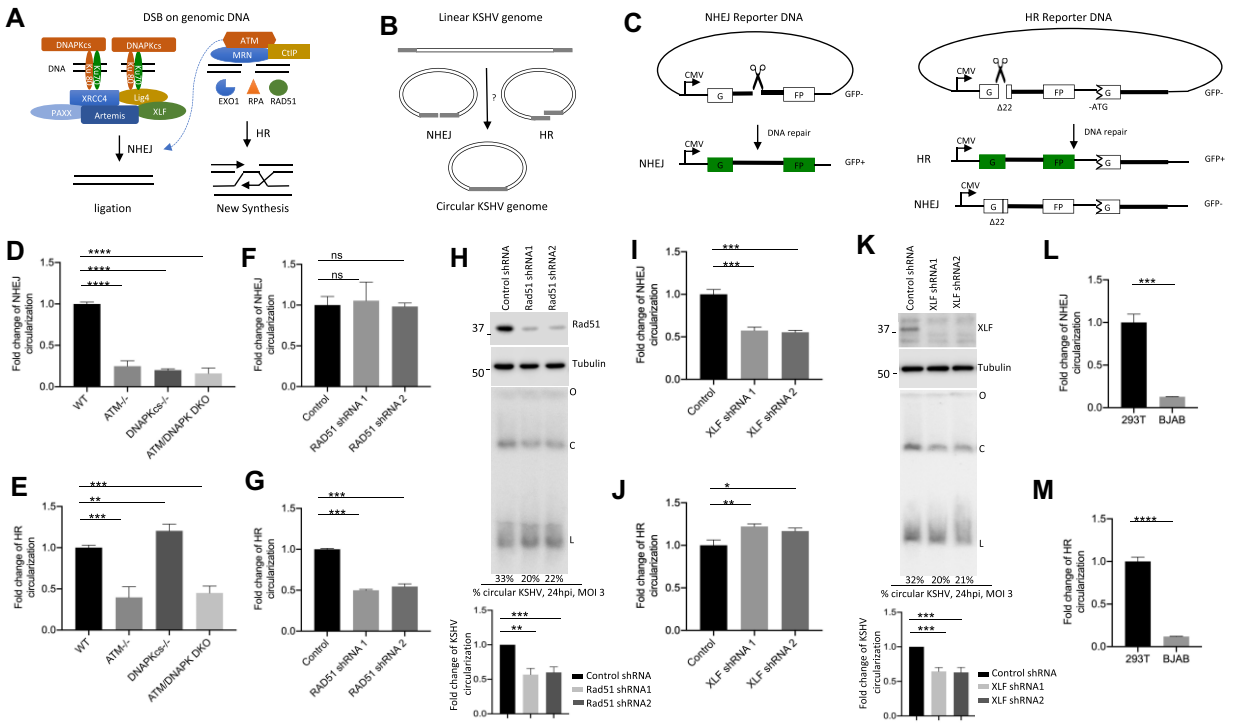

Figure 7. Both the HR and NHEJ DSB repair pathways have roles in KSHV circularization. (**A**) Schematic diagram of the NHEJ and HR DSB repair pathways. (**B**) Schematic diagram showing hypothesized NHEJ or HR mediated KSHV circularization. KSHV terminal repeat elements of KSHV genome are shown in gray. (**C**) Schematic diagram of the NHEJ and HR reporters. Reporter DNA is linearized by SceI digestion prior to transfection into cells and expresses GFP only after circularization by the designated pathway. HR reporter DNA does not express GFP if ligated by NHEJ due to a deletion (Δ22) that shifts the open reading frame. (**D**) NHEJ reporter circularization in ATM-/-, DNAPKcs-/-, or ATM/DNAPKcs double KO cells relative to that of WT cells. Two independent cell lines for each mutant derived from two different sgRNAs were used for analysis. (**E**) HR reporter DNA circularization in WT, ATM-/-, DNAPKcs-/-, or ATM/DNAPKcs double KO cells. Two independent cell lines for each mutant derived from two different sgRNAs were used for analysis. (**F**) NHEJ reporter DNA circularization in WT or Rad51 deficient cells. Two independent Rad51 deficient cell lines derived from two different shRNAs were used for analysis. (**G**) HR reporter DNA circularization in WT or Rad51 deficient cells. (**H**) Top, immunoblot of Rad51; middle, Gardella gel following rKSHV.219 infection of cells with control or Rad51 shRNA knockdown; bottom, fold change circularization from three independent experiments (shown in Supplementary Figure S9). (**I**) NHEJ reporter DNA circularization in WT or XLF deficient cells. Two independent XLF deficient cell lines derived from two different shRNAs were used for analysis. (**J**) HR reporter DNA circularization in WT or XLF deficient cells. (**K**) Top, immunoblot of XLF; middle, Gardella gel following rKSHV.219 infection of cells with control or XLF shRNA knockdown; bottom, fold change circularization from three independent experiments (shown in Supplementary Figure S11). (**L**) NHEJ reporter DNA circularization in 293T cells or BJAB cells. (**M**) HR reporter DNA circularization in 293T cells or BJAB cells. D, E, F, G, H, I, J, K, L, M means are from at least three independent experiments. Standard deviation is shown. ns, $P > 0.05$; * $P < 0.05$, ** $P < 0.01$, *** $P < 0.001$; **** $P < 0.0001$ by unpaired *t* test.

As expected, Rad51 knockdown had no effect on NHEJ, but induced HR deficiency (Figure 7F, G, Supplementary Figure S8). Following infection with rKSHV.219, circularization was modestly reduced (~20–40% less circularized band signal compared to control shRNA, as well as lower circular fraction of viral genome) in RAD51 deficient cells (Figure 7H, Supplementary Figure S9). Therefore, HR exerts a role in KSHV circularization.

We also assessed the role of the NHEJ factor, XRCC4-like factor (XLF). XLF interacts with Ligase IV to stimulate its ligase activity and forms DNA binding filaments of alternating XRCC4 and XLF dimers to allow ligation of DNA ends (52). Similar to knockout of DNAPKcs, shRNA knockdown of XLF decreased NHEJ but enhanced HR (Figure 7I, J, Supplementary Figure S10), indicating XLF is important for NHEJ, but not HR. rKSHV.219 circularization was reduced (~35–40% less circularized band signal compared to control shRNA, as well as lower circular fraction of viral genome) in XLF deficient cells (Figure 7K, Supplementary Figure S11), further supporting a role for NHEJ in virus circularization.

Since viral circularization was much more efficient in 293T than in BJAB cells (Figure 1B), we assessed whether this deficiency in circularization might relate to inefficient BJAB DDR repair mechanisms. We found BJAB cells were highly deficient for both NHEJ and HR (Figure 7L, M, Supplementary Figure S12), suggesting these deficiencies underlie inefficient KSHV circularization in these cells.

ATM and DNAPKcs are critical for HSV circularization

Since ATM and DNAPK have roles in KSHV circularization, we asked if these enzymes might also be involved in circularization of other herpesviruses, and therefore, extended our investigation to the alpha herpesvirus HSV-1. The circularization of WT HSV-1 KOS in permissive cells is not detectable by Gardella gel due to expression of the HSV ICP0, but circularization is detectable in ICP0 null virus (26). We infected 293T cells with HSV-1 KOS n212 (HSV n212) virus which contains a nonsense mutation at the ICP0 codon 212, and is therefore null for ICP0 (34,53). Following infection of ATM KO cells, circularization efficiency was modestly reduced (~40% less circularized band signal compared to WT, as well as lower circular fraction of viral genome) (Figure

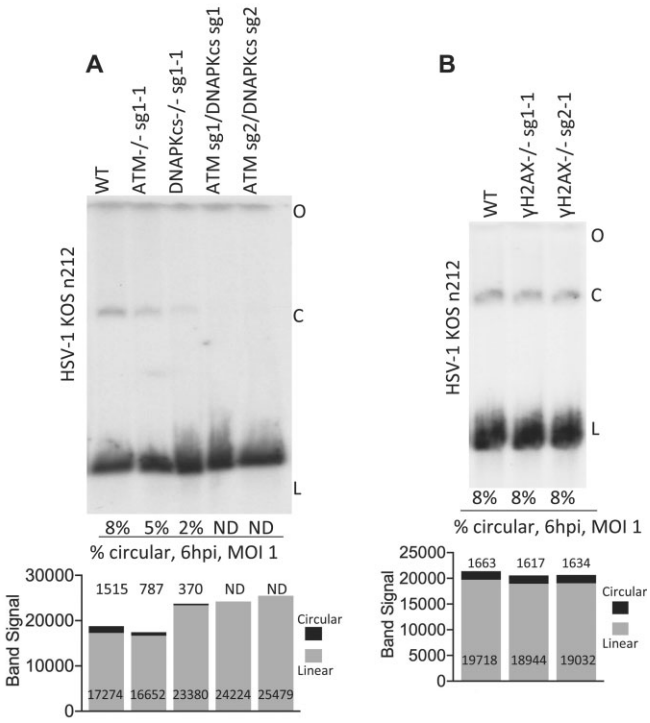

Figure 8. ATM and DNAPKcs, but not γH2AX, are involved in HSV n212 circularization. (**A**) Gardella gel following infection with HSV-1 ICP0 null (n212) in ATM-/-, DNAPKcs-/- or ATM/DNAPKcs double KO cells. Results representative of 2 independent experiments. Percent circularization and band signal intensity are shown at bottom. (**B**) Gardella gel following HSV-1 n212 infection of WT or γH2AX-/- cells. Results representative of two independent experiments. Percent circularization and band signal intensity are shown at bottom. ND, not detected.

8A, Supplementary Figure S13A) compared to WT cells, while infection of DNAPKcs KO cells resulted in a greater deficit of circularization (~75% less circularized band signal compared to WT, and also lower circular fraction of viral genome) (Figure 8A; Supplementary Figure S13A) at 6 hpi. Absence of both ATM and DNAPKcs resulted in severe circularization deficiency (Figure 8A; Supplementary Figure S13A) with no circularized forms detected.

We also assessed the role of γH2AX in HSV1 n212 circularization. Following infection, Gardella gel analysis revealed that HSV circularization in γH2AX-/- cells was similar to that in WT cells (Figure 8B; Supplementary Figure S13B), indicating it does not exert a role in HSV1 circularization.

Discussion

Following infection, KSHV dsDNA linear viral genomes are delivered to the host cell nucleus and are circularized by fusion of their free ends. Here, we show that viral DNA circularization occurs within 160′ of infection, and does not require viral protein expression (Figure 2). We also show that ATM and DNAPKcs have roles in circularizing KSHV genomes, with loss of both ATM and DNAPKcs engendering severe deficiency in circularization, and that NHEJ and HR repair mechanisms both function in circularization. In addition, ATM and DNAPKcs are important for circularization of HSV-1 (KOSn212) that is abolished for ICP0 expression (Figure 8). Since Gardella gels identify covalently closed, circular, DNA, (35) the DDR may also repair any viral genomic gaps and/or nicks in addition to fusion of DNA ends into a circle.

Host circularization of foreign, linear DNA is an intrinsic, non-specific, DDR function, as suggested by circularization of linearized NHEJ and HR plasmid reporter vectors (Figure 7). It is possible that, in response, pathogens with linear genomes, such as herpesviruses, evolved mechanisms to adapt to, and even exploit circularization, leading to a topology compatible with extrachromosomal persistence. Other viruses that undergo DDR induced genome circularization include HIV (54–57), adeno associated virus (58), and mycobacteriophage (59). In the case of herpesviruses, circularization leads to the viral episome, a key step through which latency is established (39).

Our data are consistent with a critical role for KSHV circularization in latency establishment. ATM has previously been suggested to exert a role in latency establishment. (19) Knockout of ATM, and/or DNAPKcs, resulted in circularization defects, and severity of circularization deficiency correlated with deficits in latency establishment (Figures 3, 4). In addition, in contrast to 293T cells which are highly efficient for circularization and latency establishment, BJAB cells are highly deficient for these functions (Figure 1), further suggesting a link between efficiency of circularization and latency. Once circularization is established in BJAB cells, robust episomal signal can be observed following latency establishment (Figure 1D), indicating an efficient circularization mechanism is not necessary to maintain latency following circular episome formation.

Similar to findings with KSHV, HSV circularization occurs rapidly and does not require viral gene expression (26,41). Rapid circularization is likely a common feature of herpesviruses, as another herpesvirus, varicella, also circularizes shortly after infection (60). Prior work has suggested a role for the DDR in HSV circularization. Experiments revealed reduction of formation of 'endless' HSV genomes with DNA ligase IV and XRCC4 depletion, consistent with an NHEJ effect. Such 'endless' genomes could be either from circular forms, or genome concatemers. (61) The HSV ICP0 protein may have a role in circularization, but descriptions conflict with ICP0 inhibiting circularization in one report, (26) but not in another. (62) Whether HSV uses rolling circle replication is also unclear, with some work suggesting an absence of rolling circles(26), while other results support such a model (40,62).

Despite γH2AX's expansive deposition and role in the repair of DSBs, and its presence on the KSHV genome, (20) it was dispensable for both KSHV and HSV circularization (Figure 6B, Figure 8B). However, γH2AX did exert a role in KSHV latency establishment, which was reduced about 50% compared to WT cells. Consistent with these findings, knockdown of γH2AX in primary endothelial cells resulted in a reduction of KSHV DNA copy number at 48 hpi. (19) Therefore, γH2AX is dispensable for KSHV and HSV genome circularization, but exerts a role in KSHV latency establishment.

Findings here that ATM exerts a role in NHEJ are consistent with prior reports. ATM mediates DNAPKcs phosphorylation at threonine 2609 and at adjacent (S/T)Q motifs within this threonine 2609 'cluster.' This ATM-

mediated phosphorylation is required for full activity of DNAPK and DSB repair (47,48). ATM also phosphorylates the major NHEJ DNA polymerase Polλ at threonine 204 (T204) following DSB induction with ionizing radiation. Polλ phosphorylation may enhance DSB repair and favor interaction with the DNAPK complex at DSBs (48).

Knockout of ATM induced severe deficiencies in both HR and NHEJ in a plasmid recircularization assay (Figure 7D, E), yet had only a modest effect on viral circularization (Figure 3B), suggesting KSHV largely compensates for loss of ATM or bypasses a need for it. It is possible KSHV may utilize or activate an alternative kinase or pathway to compensate for ATM deficiency, or offset a requirement for it. Since simultaneous loss of ATM and DNAPKcs led to both severe reporter plasmid and viral circularization deficiency, KSHV cannot compensate for loss of both PIKKs.

Our results indicate that both NHEJ and HR both participate in KSHV circularization. Loss of DNAPKcs or knockdown of XLF reduced both NHEJ (Figure 7D, I) and KSHV circularization (Figure 3B–D; Figure 7K), but did not diminish HR, indicating a role for NHEJ. Rad51 deficiency reduced both HR (Figure 7G) and KSHV circularization (Figure 7H), but did not reduce NHEJ (Figure 7F), indicating a role for HR. Interestingly, deficiency of DNAPKcs, XLF, or Rad51 each induced similar KSHV circularization deficiencies (∼40% less circular band signal), suggesting similar contributions for HR and NHEJ for virus circularization, at least in 293T cells. KSHV contains ∼40 identical terminal repeat elements in each genome (23,24,63), which would provide potential template for HR. In fact, evidence for homologous recombination within these repeat elements exists in KSHV LANA episome maintenance assays, which are performed in the absence of other viral genes. In these assays, transfected plasmids containing KSHV terminal repeat elements undergo recombination within these repeats (10,64–66).

In summary, ATM and DNAPKcs are important for KSHV circularization and latency establishment, and exert roles in HSV-1 n212 circularization. In addition, both HR and NHEJ contribute to KSHV circularization, a hallmark of herpesvirus latency. The development of strategies to disrupt herpesvirus circularization may potentially be an effective tool to prevent latency and herpesvirus disease.

Data availability

The data underlying this article are available in the article and in its online supplementary material.

Supplementary data

Supplementary Data are available at NAR Online.

Acknowledgements

We thank David Knipe for helpful discussions.

Funding

National Institutes of Health [AI150575, DE025208, AI165382 to K.M.K.]; J.P.S. is supported by FCT [PTDC/BIA-VIR/27947/2017]; N.V.S. is supported by T32 AI007245. Funding for open access charge: NIH.

Conflict of interest statement

None declared.

References

1. Weidner-Glunde,M., Kruminis-Kaszkiel,E. and Savanagouder,M. (2020) Herpesviral latency-common themes. *Pathogens*, **9**, 125.
2. Dupin,N., Fisher,C., Kellam,P., Ariad,S., Tulliez,M., Franck,N., van Marck,E., Salmon,D., Gorin,I., Escande,J.P., *et al.* (1999) Distribution of human herpesvirus-8 latently infected cells in Kaposi's sarcoma, multicentric Castleman's disease, and primary effusion lymphoma. *Proc. Natl. Acad. Sci. U.S.A.*, **96**, 4546–4551.
3. Dupin,N., Diss,T.L., Kellam,P., Tulliez,M., Du,M.Q., Sicard,D., Weiss,R.A., Isaacson,P.G. and Boshoff,C. (2000) HHV-8 is associated with a plasmablastic variant of Castleman disease that is linked to HHV-8-positive plasmablastic lymphoma. *Blood*, **95**, 1406–1412.
4. Cesarman,E., Chang,Y., Moore,P.S., Said,J.W. and Knowles,D.M. (1995) Kaposi's sarcoma-associated herpesvirus-like DNA sequences in AIDS-related body-cavity-based lymphomas. *NEJM*, **332**, 1186–1191.
5. Moore,P.S. and Chang,Y. (1995) Detection of herpesvirus-like DNA sequences in Kaposi's sarcoma in patients with and without HIV infection [see comments]. *N. Engl. J. Med.*, **332**, 1181–1185.
6. Oksenhendler,E., Duarte,M., Soulier,J., Cacoub,P., Welker,Y., Cadranel,J., Cazals-Hatem,D., Autran,B., Clauvel,J.P. and Raphael,M. (1996) Multicentric Castleman's disease in HIV infection: a clinical and pathological study of 20 patients. *AIDS*, **10**, 61–67.
7. Soulier,J., Grollet,L., Oksenhendler,E., Cacoub,P., Cazals-Hatem,D., Babinet,P., Agay,M.-F., Clauvel,J.-P., Raphael,M., Degos,L., *et al.* (1995) Kaposi's Sarcoma-associated herpesvirus-like DNA sequences in multicentric Castleman's disease. *Blood*, **86**, 1276–1280.
8. Decker,L.L., Shankar,P., Khan,G., Freeman,R.B., Dezube,B.J., Lieberman,J. and Thorley-Lawson,D.A. (1996) The Kaposi sarcoma-associated herpesvirus (KSHV) is present as an intact latent genome in KS tissue but replicates in the peripheral blood mononuclear cells of KS patients. *J. Exp. Med.*, **184**, 283–288.
9. Ballestas,M.E., Chatis,P.A. and Kaye,K.M. (1999) Efficient persistence of extrachromosomal KSHV DNA mediated by latency- associated nuclear antigen. *Science*, **284**, 641–644.
10. Ballestas,M.E. and Kaye,K.M. (2001) Kaposi's sarcoma-associated herpesvirus latency-associated nuclear antigen 1 mediates episome persistence through cis-acting terminal repeat (TR) sequence and specifically binds TR DNA. *J. Virol.*, **75**, 3250–3258.
11. Cotter,M.A. and Robertson,E.S. (1999) The latency-associated nuclear antigen tethers the Kaposi's sarcoma- associated herpesvirus genome to host chromosomes in body cavity-based lymphoma cells. *Virology*, **264**, 254–264.
12. Ciccia,A. and Elledge,S.J. (2010) The DNA damage response: making it safe to play with knives. *Mol. Cell*, **40**, 179–204.
13. Blackford,A.N. and Jackson,S.P. (2017) ATM, ATR, and DNA-PK: the trinity at the heart of the DNA damage response. *Mol. Cell*, **66**, 801–817.
14. Rogakou,E.P., Boon,C., Redon,C. and Bonner,W.M. (1999) Megabase chromatin domains involved in DNA double-strand breaks in vivo. *J. Cell Biol.*, **146**, 905–916.
15. Kinner,A., Wu,W., Staudt,C. and Iliakis,G. (2008) Gamma-H2AX in recognition and signaling of DNA double-strand breaks in the context of chromatin. *Nucleic Acids Res.*, **36**, 5678–5694.
16. Koopal,S., Furuhjelm,J.H., Jarviluoma,A., Jaamaa,S., Pyakurel,P., Pussinen,C., Wirzenius,M., Biberfeld,P., Alitalo,K., Laiho,M., *et al.* (2007) Viral oncogene-induced DNA damage response is activated in Kaposi sarcoma tumorigenesis. *PLoS Pathog.*, **3**, 1348–1360.
17. Hollingworth,R., Skalka,G.L., Stewart,G.S., Hislop,A.D., Blackbourn,D.J. and Grand,R.J. (2015) Activation of DNA

damage response pathways during lytic replication of KSHV. *Viruses*, **7**, 2908–2927.
18. Nikitin,P.A. and Luftig,M.A. (2012) The DNA damage response in viral-induced cellular transformation. *Br. J. Cancer*, **106**, 429–435.
19. Singh,V.V., Dutta,D., Ansari,M.A., Dutta,S. and Chandran,B. (2014) Kaposi's Sarcoma-associated herpesvirus induces the ATM and H2AX DNA damage response early during De Novo infection of primary endothelial cells, which play roles in latency establishment. *J. Virol.*, **88**, 2821–2834.
20. Jha,H.C., Upadhyay,S.K., M,A.J.P., Lu,J., Cai,Q., Saha,A. and Robertson,E.S. (2013) H2AX phosphorylation is important for LANA-mediated Kaposi's sarcoma-associated herpesvirus episome persistence. *J. Virol.*, **87**, 5255–5269.
21. Shin,Y.C., Nakamura,H., Liang,X., Feng,P., Chang,H., Kowalik,T.F. and Jung,J.U. (2006) Inhibition of the ATM/p53 signal transduction pathway by Kaposi's sarcoma-associated herpesvirus interferon regulatory factor 1. *J. Virol.*, **80**, 2257–2266.
22. Russo,J.J., Bohenzky,R.A., Chien,M.-C., Chen,J., Yan,M., Maddalena,D., Parry,J.P., Peruzzi,D., Eman,I.S., Chang,Y., *et al.* (1996) Nucleotide sequence of the Kaposi sarcoma-associated herpesvirus (HHV8). *Proc. Natl Acad. Sci. U.S.A.*, **93**, 14862–14867.
23. Judde,J.G., Lacoste,V., Briere,J., Kassa-Kelembho,E., Clyti,E., Couppie,P., Buchrieser,C., Tulliez,M., Morvan,J. and Gessain,A. (2000) Monoclonality or oligoclonality of human herpesvirus 8 terminal repeat sequences in Kaposi's sarcoma and other diseases. *J. Natl. Cancer Inst.*, **92**, 729–736.
24. Duprez,R., Lacoste,V., Briere,J., Couppie,P., Frances,C., Sainte-Marie,D., Kassa-Kelembho,E., Lando,M.J., Essame Oyono,J.L., Nkegoum,B., *et al.* (2007) Evidence for a multiclonal origin of multicentric advanced lesions of Kaposi sarcoma. *J. Natl. Cancer Inst.*, **99**, 1086–1094.
25. Luftig,M.A. (2014) Viruses and the DNA damage response: activation and antagonism. *Annu. Rev. Virol.*, **1**, 605–625.
26. Jackson,S.A. and DeLuca,N.A. (2003) Relationship of herpes simplex virus genome configuration to productive and persistent infections. *Proc. Natl. Acad. Sci. U.S.A.*, **100**, 7871–7876.
27. Canman,C.E., Lim,D.S., Cimprich,K.A., Taya,Y., Tamai,K., Sakaguchi,K., Appella,E., Kastan,M.B. and Siliciano,J.D. (1998) Activation of the ATM kinase by ionizing radiation and phosphorylation of p53. *Science*, **281**, 1677–1679.
28. Cui,X., Yu,Y., Gupta,S., Cho,Y.M., Lees-Miller,S.P. and Meek,K. (2005) Autophosphorylation of DNA-dependent protein kinase regulates DNA end processing and may also alter double-strand break repair pathway choice. *Mol. Cell. Biol.*, **25**, 10842–10852.
29. Douglas,P., Cui,X., Block,W.D., Yu,Y., Gupta,S., Ding,Q., Ye,R., Morrice,N., Lees-Miller,S.P. and Meek,K. (2007) The DNA-dependent protein kinase catalytic subunit is phosphorylated in vivo on threonine 3950, a highly conserved amino acid in the protein kinase domain. *Mol. Cell. Biol.*, **27**, 1581–1591.
30. Stringer,B.W., Day,B.W., D'Souza,R.C.J., Jamieson,P.R., Ensbey,K.S., Bruce,Z.C., Lim,Y.C., Goasdoue,K., Offenhauser,C., Akgul,S, *et al.* (2019) A reference collection of patient-derived cell line and xenograft models of proneural, classical and mesenchymal glioblastoma. *Sci. Rep.*, **9**, 4902.
31. Stewart,S.A., Dykxhoorn,D.M., Palliser,D., Mizuno,H., Yu,E.Y., An,D.S., Sabatini,D.M., Chen,I.S., Hahn,W.C., Sharp,P.A., *et al.* (2003) Lentivirus-delivered stable gene silencing by RNAi in primary cells. *RNA*, **9**, 493–501.
32. Seluanov,A., Mao,Z. and Gorbunova,V. (2010) Analysis of DNA double-strand break (DSB) repair in mammalian cells. *J. Visual. Exp.***43**, 2002.
33. Myoung,J. and Ganem,D. (2011) Generation of a doxycycline-inducible KSHV producer cell line of endothelial origin: maintenance of tight latency with efficient reactivation upon induction. *J. Virol. Methods*, **174**, 12–21.
34. Cai,W.Z. and Schaffer,P.A. (1989) Herpes simplex virus type 1 ICP0 plays a critical role in the de novo synthesis of infectious virus following transfection of viral DNA. *J. Virol.*, **63**, 4579–4589.
35. Gardella,T., Medveczky,P., Sairenji,T. and mulder,C. (1984) Detection of circular and linear herpesvirus DNA molecules in mammalian cells by gel electrophoresis. *J. Virol.*, **50**, 248–254.
36. Vieira,J. and O'Hearn,P.M. (2004) Use of the red fluorescent protein as a marker of Kaposi's sarcoma-associated herpesvirus lytic gene expression. *Virology*, **325**, 225–240.
37. Grundhoff,A. and Ganem,D. (2004) Inefficient establishment of KSHV latency suggests an additional role for continued lytic replication in Kaposi sarcoma pathogenesis. *J. Clin. Invest.*, **113**, 124–136.
38. Zhong,W., HaoWang,H. and Ganem,D. (1996) Restricted expression of Kaposi sarcoma-associated herpesvirus (human herpesvirus 8) genes in Kaposi sarcoma. *Proc. Natl Acad. Sci.*, **93**, 6641–6646.
39. Damiania,B. and Cesarman,E. (2022) In: Howley,P.M., Knipe,D.M., Damania,B., Cohen,J.I., Whelan,S.P.J., Enquist,L. and Freed,E.O. (eds.) *Fields Virology: DNA Viruses*. 7th edn., Wolters Kluwer, NY, pp. 513–572.
40. Poffenberger,K.L. and Roizman,B. (1985) A noninverting genome of a viable herpes simplex virus 1: presence of head-to-tail linkages in packaged genomes and requirements for circularization after infection. *J. Virol.*, **53**, 587–595.
41. Garber,D.A., Beverley,S.M. and Coen,D.M. (1993) Demonstration of circularization of herpes simplex virus DNA following infection using pulsed field gel electrophoresis. *Virology*, **197**, 459–462.
42. Foreman,K.E., Bacon,P.E., Hsi,E.D. and Nickoloff,B.J. (1997) In situ polymerase chain reaction-based localization studies support role of human herpesvirus-8 as the cause of two AIDS-related neoplasms: kaposi's sarcoma and body cavity lymphoma. *J. Clin. Invest.*, **99**, 2971–2978.
43. Pauk,J., Huang,M.L., Brodie,S.J., Wald,A., Koelle,D.M., Schacker,T., Celum,C., Selke,S. and Corey,L. (2000) Mucosal shedding of Human herpesvirus 8 in men. *N. Engl. J. Med.*, **343**, 1369–1377.
44. Stiff,T., O'Driscoll,M., Rief,N., Iwabuchi,K., Lobrich,M. and Jeggo,P.A. (2004) ATM and DNA-PK function redundantly to phosphorylate H2AX after exposure to ionizing radiation. *Cancer Res.*, **64**, 2390–2396.
45. Graham,T.G., Walter,J.C. and Loparo,J.J. (2016) Two-stage synapsis of DNA ends during non-homologous end joining. *Mol. Cell*, **61**, 850–858.
46. Shiloh,Y. (2003) ATM and related protein kinases: safeguarding genome integrity. *Nat. Rev. Cancer*, **3**, 155–168.
47. Chen,B.P., Uematsu,N., Kobayashi,J., Lerenthal,Y., Krempler,A., Yajima,H., Lobrich,M., Shiloh,Y. and Chen,D.J. (2007) Ataxia telangiectasia mutated (ATM) is essential for DNA-PKcs phosphorylations at the thr-2609 cluster upon DNA double strand break. *J. Biol. Chem.*, **282**, 6582–6587.
48. Sastre-Moreno,G., Pryor,J.M., Moreno-Onate,M., Herrero-Ruiz,A.M., Cortes-Ledesma,F., Blanco,L., Ramsden,D.A. and Ruiz,J.F. (2017) Regulation of human pollambda by ATM-mediated phosphorylation during non-homologous end joining. *DNA Repair (Amst.)*, **51**, 31–45.
49. Seluanov,A., Mittelman,D., Pereira-Smith,O.M., Wilson,J.H. and Gorbunova,V. (2004) DNA end joining becomes less efficient and more error-prone during cellular senescence. *Proc. Natl. Acad. Sci. U.S.A.*, **101**, 7624–7629.
50. Mao,Z., Seluanov,A., Jiang,Y. and Gorbunova,V. (2007) TRF2 is required for repair of nontelomeric DNA double-strand breaks by homologous recombination. *Proc. Natl. Acad. Sci. USA*, **104**, 13068–13073.
51. Jasin,M. and Rothstein,R. (2013) Repair of strand breaks by homologous recombination. *Cold Spring Harb. Perspect. Biol.*, **5**, a012740.
52. Menon,V. and Povirk,L.F. (2017) XLF/Cernunnos: an important but puzzling participant in the nonhomologous end joining DNA repair pathway. *DNA Repair (Amst.)*, **58**, 29–37.

53. Cai,W., Astor,T.L., Liptak,L.M., Cho,C., Coen,D.M. and Schaffer,P.A. (1993) The herpes simplex virus type 1 regulatory protein ICP0 enhances virus replication during acute infection and reactivation from latency. *J. Virol.*, **67**, 7501–7512.
54. Jeanson,L. and Mouscadet,J.F. (2002) Ku represses the HIV-1 transcription: identification of a putative Ku binding site homologous to the mouse mammary tumor virus NRE1 sequence in the HIV-1 long terminal repeat. *J. Biol. Chem.*, **277**, 4918–4924.
55. Kilzer,J.M., Stracker,T., Beitzel,B., Meek,K., Weitzman,M. and Bushman,F.D. (2003) Roles of host cell factors in circularization of retroviral dna. *Virology*, **314**, 460–467.
56. Li,L., Olvera,J.M., Yoder,K.E., Mitchell,R.S., Butler,S.L., Lieber,M., Martin,S.L. and Bushman,F.D. (2001) Role of the non-homologous DNA end joining pathway in the early steps of retroviral infection. *EMBO J.*, **20**, 3272–3281.
57. Skalka,A.M. and Katz,R.A. (2005) Retroviral DNA integration and the DNA damage response. *Cell Death Differ.*, **12**(Suppl. 1), 971–978.
58. Choi,V.W., McCarty,D.M. and Samulski,R.J. (2006) Host cell DNA repair pathways in adeno-associated viral genome processing. *J. Virol.*, **80**, 10346–10356.
59. Pitcher,R.S., Tonkin,L.M., Daley,J.M., Palmbos,P.L., Green,A.J., Velting,T.L., Brzostek,A., Korycka-Machala,M., Cresawn,S., Dziadek,J., *et al.* (2006) Mycobacteriophage exploit NHEJ to facilitate genome circularization. *Mol. Cell*, **23**, 743–748.
60. Kinchington,P.R., Reinhold,W.C., Casey,T.A., Straus,S.E., Hay,J. and Ruyechan,W.T. (1985) Inversion and circularization of the varicella-zoster virus genome. *J. Virol.*, **56**, 194–200.
61. Muylaert,I. and Elias,P. (2007) Knockdown of DNA ligase IV/XRCC4 by RNA interference inhibits herpes simplex virus type I DNA replication. *J. Biol. Chem.*, **282**, 10865–10872.
62. Strang,B.L. and Stow,N.D. (2005) Circularization of the herpes simplex virus type 1 genome upon lytic infection. *J. Virol.*, **79**, 12487–12494.
63. Lagunoff,M. and Ganem,D. (1997) The structure and coding organization of the genomic termini of Kaposi's sarcoma-associated herpesvirus (Human Herpesvirus 8). *Virology*, **236**, 147–154.
64. De Leon Vazquez,E., Carey,V.J. and Kaye,K.M. (2013) Identification of Kshv Lana regions important for episome segregation, replication and persistence. *J. Virol.*, **87**, 12270–12283.
65. De Leon Vazquez,E., Juillard,F., Rosner,B. and Kaye,K.M. (2014) A short sequence immediately upstream of the internal repeat elements is critical for KSHV LANA mediated DNA replication and impacts episome persistence. *Virology*, **448**, 344–355.
66. Habison,A.C., Beauchemin,C., Simas,J.P., Usherwood,E.J. and Kaye,K.M. (2012) Murine gammaherpesvirus 68 LANA acts on terminal repeat DNA to mediate episome persistence. *J. Virol.*, **86**, 11863–11876.

Received: October 16, 2023. **Revised:** December 5, 2023. **Editorial Decision:** December 8, 2023. **Accepted:** December 16, 2023